# ChemComm

Check for updates

# The advent and development of organophotoredox catalysis

Tommaso Bortolato, [iD] Sara Cuadros, Gianluca Simionato and Luca Dell'Amico [iD] *

In the last decade, photoredox catalysis has unlocked unprecedented reactivities in synthetic organic chemistry. Seminal advancements in the field have involved the use of well-studied metal complexes as photoredox catalysts (PCs). More recently, the synthetic community, looking for more sustainable approaches, has been moving towards the use of purely organic molecules. Organic PCs are generally cheaper and less toxic, while allowing their rational modification to an increased generality. Furthermore, organic PCs have allowed reactivities that are inaccessible by using common metal complexes. Likewise, in synthetic catalysis, the field of photocatalysis is now experiencing a green evolution moving from metal catalysis to organocatalysis. In this feature article, we discuss and critically comment on the scientific reasons for this ongoing evolution in the field of photoredox catalysis, showing how and when organic PCs can efficiently replace their metal counterparts.

## 1 From photochemistry to synthetic photoredox catalysis

Photochemistry is a branch of chemistry that deals with the chemical effects of light.[1] Upon light-irradiation, organic molecules can reach an electronically excited state whose reactivity and physicochemical properties are substantially different from those

*Department of Chemical Sciences, University of Padova, Via Marzolo 1, Padova, 35131, Italy. E-mail: luca.dellamico@unipd.it*

in the ground state. We can track back the first observation of the effect of light on organic molecules in 1834 when the German chemist Johann Bartholomew Trommsdorff discovered that Santonin, an anthelmintic sesquiterpene lactone, photoisomerises upon irradiation with blue and violet light.[2] However, it is since the 20th century, thanks to the work of Ciamician and Silber, that photochemistry has been considered a major branch of chemistry worth systematic investigations.[3]

The earliest examples of photochemical transformations involved the direct irradiation of substrates. Nowadays, the



**From right to left: Tommaso Bortolato, Gianluca Simionato, Luca Dell'Amico and Sara Cuadros**

*Tommaso Bortolato graduated in Chemistry in 2019 from the University of Padova (Italy). In 2020, he started his PhD in Luca Dell'Amico's group focusing on the development of novel sustainable light-driven methods. Gianluca Simionato completed his MSc in Industrial Chemistry in 2021 at the University of Padova under the supervision of Dr Luca Dell'Amico. His current research deals with the design and study of new heterocyclic organophotoredox catalysts. Luca Dell'Amico completed his PhD at the University of Parma (Italy), under the supervision of Prof. Franca Zanardi, in 2014. He spent a research period with Prof. Karl Anker Jørgensen at Århus University (Denmark), where he was introduced to the field of organocatalysis. From 2014 to 2016, he was a Marie Curie fellow in Prof. Paolo Melchiorre's group at ICIQ (Spain). In 2017, he started his independent career at the University of Padova. His research targets the development and mechanistic investigation of novel photochemical processes. Sara Cuadros graduated from the University of Alicante in* 2014. She obtained her MSc and PhD degrees in 2019, under the supervision of Prof. Paolo Melchiorre at ICIQ (Spain). She is currently a postdoctoral researcher at the University of Padova. Her research focuses on the synthesis of novel PET radioligands for functional imaging.
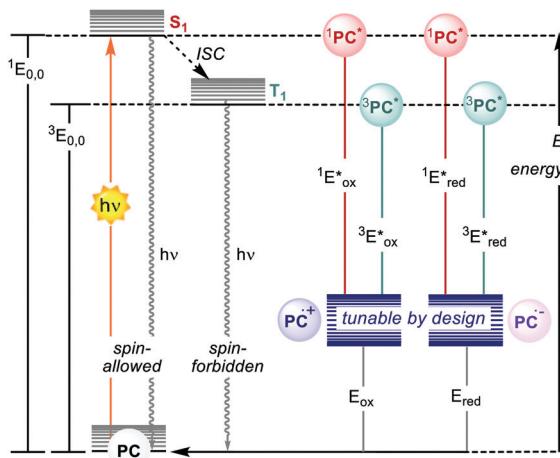
**Fig. 1** Schematic representation of the ground- and excited-states and electrochemical properties of PCs.

most general and rapidly evolving branch of synthetic photo-chemistry is photoredox catalysis.

Photoredox catalysis makes use of a light-absorbing molecule, the photoredox catalyst (PC): an organometallic complex, an organic molecule or a material which harvests light reaching an electronically excited state (Fig. 1). The $S_1$ singlet excited state can either decay through fluorescence or relax to a triplet $T_1$ state with lower energy through intersystem crossing (ISC). The $T_1$ state can then decay through phosphorescence, which, however, is a spin-forbidden process. Thus, the $T_1$ state is typically longer-lived than the $S_1$ state. The PC in the excited state ($S_1$ or $T_1$) is a stronger oxidant and reductant than in the ground state. The redox potentials in the excited state are determined by the ground-state redox potentials and the energy of the involved excited state $E_{0,0}$ (Fig. 1).[4]

The interaction between the excited-state PC (PC*) and an electron-donor (*D*) or electron-acceptor (*A*) leads to a redox event known as *photoinduced electron transfer* (PET). Its nature depends on the thermodynamic and kinetic feasibility.

Classically, a PET in which the PC acts as the reductant getting oxidised is called *oxidative quenching* (left pathway, Scheme 1).

On the other hand, we consider a *reductive quenching* if the PC gets reduced (right pathway, Scheme 1). Through a PET process, it is possible to generate a radical species under mild conditions, using visible light as the only (or the main) energy source.
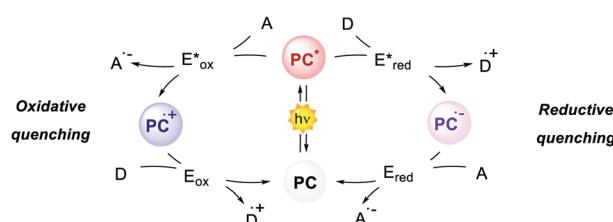


**Scheme 1** General mechanisms of oxidative and reductive quenching. D = donor; A = acceptor.

The earliest example of photoredox catalysis in organic synthesis dates back to 1978 when Kellogg observed that the reduction of phenacyl sulfonium salts by 1,4-dihydropyridines was greatly accelerated under visible light irradiation in the presence of a catalytic amount of $Ru(bpy)_3Cl_2$ or eosin.[5a] Subsequent studies in the 1980s[5b–e] and early 1990s[5f–h] contributed to establishing the foundations of modern photo-redox catalysis. Between 2008 and 2009, the pioneering reports by Yoon's,[6] MacMillan's[7] and Stephenson's[8] groups fully disclosed the tremendous potential of photoredox catalysis when applied to organic synthesis. Since then, the field has been steadily growing year by year (Fig. 2).[9]

## 2 Metal-based photoredox catalysis

Until recently, Ru- and Ir-based PCs have dominated the field of synthetic photoredox catalysis (Scheme 2). $Ru(bpy)_3{}^{2+}$ **1a** has the longest history as a PC. It has been largely used for applications such as water splitting[10] and carbon dioxide reduction.[11] The balanced excited-redox potentials of **1a** make it able to engage in both oxidative and reductive quenching processes.[12] Similarly, *fac*-Ir(ppy)$_3$ **2a** is another transition metal-based PC that has been extensively used in photoredox catalysis. It is a strongly reducing PC,[13] with long-standing emission, ideal to be used in organic light emitting diodes (OLEDs).[14] The excited state of **2a** is about 500 mV less oxidising and 900 mV more reducing than **1a** (Scheme 2).[15]

Upon light absorption in the blue region, **1a** and **2a** get promoted to the $S_1$ state. The $S_1$ state efficiently undergoes ISC to the lower $T_1$ state.[15] Both states are involved in an intramolecular metal-to-ligand charge transfer (MLCT) from an electron-donating ligand to the electron-accepting metal centre. The $S_1$ and $T_1$ states are thus named $^1$MLCT and $^3$MLCT, respectively.

The popularity of Ru- and Ir-based complexes can be ascribed to a combination of two main factors. First, the photophysical properties of some Ru- and Ir-based complexes have been known for decades. Hence, the synthetic community has benefited from an extensive set of physicochemical data already available. Second, Ru- and Ir-based PCs undergo an efficient ISC to the $T_1$ state. The population of the $T_1$ state produces a long-lived excited state further extended by the MLCT. Such a long-lived excited state (in the order of the μs) facilitates the interaction with the substrate, thus favouring the PET.

Metal complexes have a complex set of excited states.[15] Their relative energetic ordering and their photophysics depend on the intrinsic properties of metal and ligands. As a result, the rational fine-tuning of the redox properties of Ru and Ir PCs by ligand modification is particularly complex.[16,17] A simple variation on the electronics of the ligand(s) affects the photophysics of the PC (Scheme 2).[18] Additionally, the introduction of electron-donating groups into the ligand(s) has little or no effect on the redox potentials.[19,20]

Transition metal PCs are not the ideal options from a sustainable perspective. Both ruthenium and iridium have an abundance of around 0.001 ppm on the Earth's crust and are
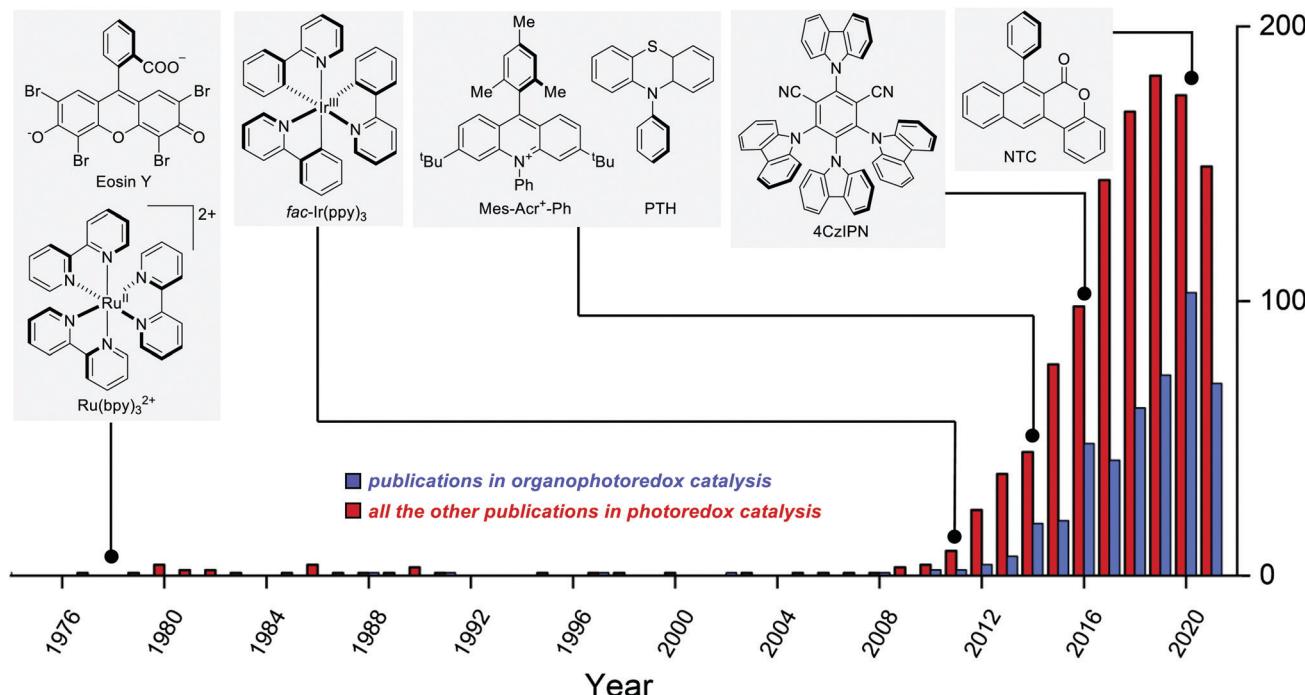
**Fig. 2** Graphical depiction of the number of articles published each year in the fields of synthetic photoredox catalysis. The blue columns depict the contribution of organophotoredox catalysis to the total, while the red columns depict the rest of the published papers. The structures of selected PCs are linked to the year of their first use in synthetic chemistry.
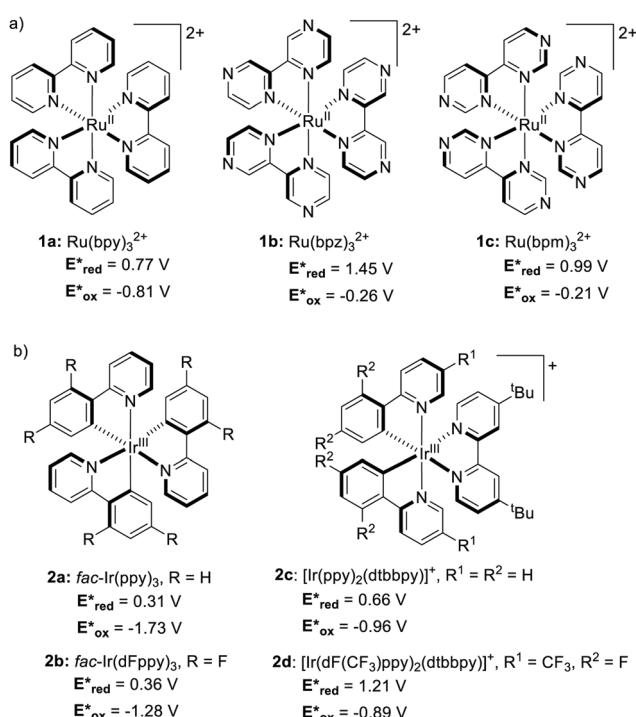
**Scheme 2** Structures and excited-state redox potentials (*vs.* SCE in MeCN) of the selected (a) Ru and (b) Ir complexes (ref. 15).

thus among the rarest metals.[21] This issue also impacts their high prices, hampering their massive use in the future.[22]

For this reason, the community has evaluated the possibility of using more abundant metals, such as iron. However, the longest-lived excited state for a Fe$^{II}$ complex is in the order of 100 ps, while the typical lifetimes of Ru- and Ir-based PCs reach several μs.[23] This is because the coordination of a metal with the ligands provides an energy splitting ($\Delta E$) between the ground state and the triplet metal-centred $^3$MC state. If the $\Delta E$ is small enough, the excited state that gets populated is the $^3$MC state (Fig. 3a). This $^3$MC state is non-emissive and gets rapidly deactivated by nonradiative decay, being thus unable to engage in PET. Conversely, a large $\Delta E$ brings the $^3$MC state so
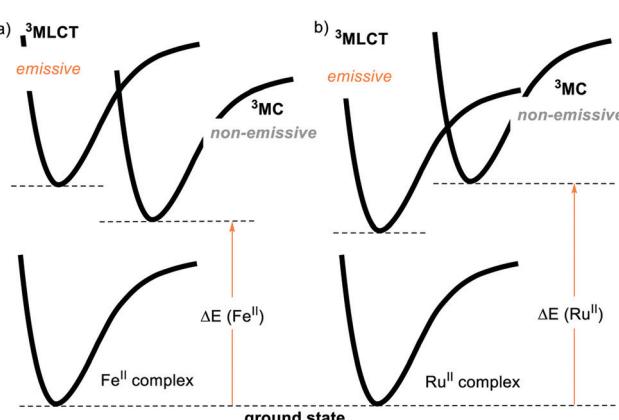


**Fig. 3** Schematic representation of the metal-to-ligand-charge transfer ($^3$MLCT), metal-centred ($^3$MC) and ground states (GS) energy levels for (a) Fe$^{II}$ and (b) Ru$^{II}$ complexes.

high in energy that the $^3$MLCT level becomes populated (Fig. 3b).[14] Since the second- and third-row transition metals typically have a larger $\Delta E$ compared to their first-row counterparts, the development of abundant first-row metal complexes as PCs is much more challenging.[24a] On the other hand, Cu-complexes have given promising results.[24b,c]

# 3 Organic photoredox catalysts

Over the last few years, the development and use of purely organic photoredox catalysts have seen a rapid increase (Fig. 2), as witnessed by the increasing number of papers and reviews on the topic.[25] Many organic dyes have been known for a long time, but their synthetic potential has been disclosed only recently.

The need for more sustainable catalytic systems and predictable PC properties has prompted recent research towards organic molecules. In contrast to metal complexes, the structure–property relationships and rational design of organic PCs are highly simplified.[26]

Upon light irradiation, an organic PC is promoted to its excited $S_1$ state, generally through a $\pi-\pi^*$ transition. The $S_1$ state has a lifetime in the order of ns, and it is usually the state involved in the redox event. However, in some cases, a $T_1$ state is reached by ISC.[27] In the $S_1$ state, the redox potential window is dictated by the $^1E_{0,0}$ with none or minor energy loss (refer to Fig. 1).[4] Similarly, the redox potential window of the $T_1$ state is dictated by the $^3E_{0,0}$, which is lower than $^1E_{0,0}$ due to the energy lost through the ISC. The main advantage of the $T_1$ state is its longer lifetime, kinetically desirable for PET processes. While Ru- and Ir-based PCs always populate the $T_1$ state with high efficiency, organic PCs can be rationally designed to operate through the $S_1$ or the $T_1$ state.

Analogously to the MLCT character in metal-based PCs, in organic PCs, a charge-transfer (CT) character in the excited state is accessed when the HOMO and LUMO are spatially separated.[26b] The CT state is useful to increase the excited state lifetime.[28] The effect of the CT character on the lifetime is often dramatic. For instance, considering 9,10-dicyanoanthracene (**3a**) and 4CzTPN, **3b**. The first has a lifetime of 14.9 ns, while the second experiences a $> 100$-fold increase, due to the strong CT character of its excited state (Fig. 4).[25l]

Another advantage of having spatially separated HOMO and LUMO is the possibility to independently alter the energy of the
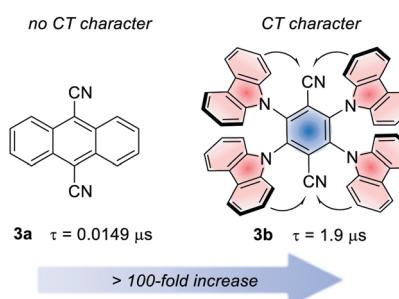


Fig. 5 Selected examples of extremely oxidising and reducing PCs. Potentials *vs.* SCE in MeCN.

two levels by introducing electron-donating or electron-withdrawing substituents in a specific position of the molecule. This strategy allows tailoring the ground-state and excited-state redox potentials of the PC, in an almost independent manner.[26] In this way, it is possible to rationally design new organic PCs with the desired characteristics.

A recent classification of organic PCs is based on their ability to activate the substrate either towards oxidation or reduction. We can thus talk about (i) strongly oxidising, (ii) strongly reducing and (iii) bimodal organic PCs (Fig. 5). Bimodal PCs have a balanced distribution of their redox power which allows their use in both oxidative and reductive quenching manifolds.

# 4 Unveiling the potential of organic PCs in photoredox catalysis – a comparative analysis

## 4.1 Replacement of a Ru-complex for an organic PC

Ru(bpy)$_3$$^{2+}$ **1a** absorbs visible photons ($\lambda_{max}$ = 452 nm), giving access to a long-lived triplet $^3$MLCT state ($\tau$ = 1.1 μs).[15] Thus, this metal-based PC can participate in both oxidative ($E^*_{ox}$ = $-0.81$ V *vs.* SCE in MeCN) and reductive quenching processes ($E^*_{red}$ = $+0.77$ V *vs.* SCE in MeCN) (Scheme 3).[11] Nevertheless, its relatively narrow redox potential window has hampered the use of this catalyst for the activation of substrates with high thermodynamic requirements. Likewise, eosin Y **4** (EY, Scheme 4) exhibits a narrow redox window and similar redox properties.[25b]

Thus, the commercially available and cheaper EY can be effectively used to replace Ru(bpy)$_3$$^{2+}$, especially for reactions proceeding through a reductive quenching mechanism.[30] Upon



Fig. 4 Example of the effect of the CT character for the PC lifetime ($\tau$).
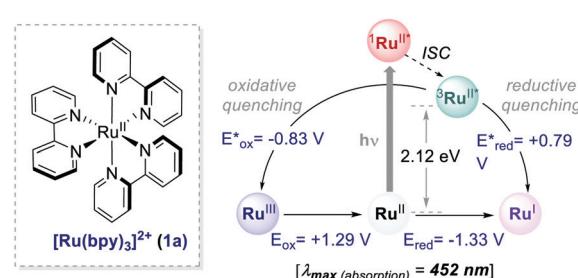


Scheme 3 Photophysical properties and redox potentials (*vs.* SCE in MeCN) of Ru(bpy)$_3$$^{2+}$ (ref. 15).
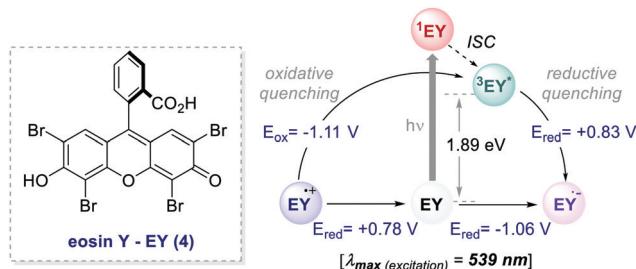
**Scheme 4** Photophysical properties and redox potentials (*vs.* SCE in 1:1 MeCN:$H_2O$) of eosin Y (ref. 25*b* and 29).

irradiation ($\lambda_{max}$ = 539 nm), EY reaches the $S_1$ state that undergoes a rapid ISC to the lowest $T_1$ state, which has a lifetime of 24 µs.[31] Additionally, this well-known organic dye[31–34] allows the use of low-energy green light, representing a milder alternative to trigger photoredox processes.

In 2011, König and Zeitler's groups reported a comparative study between the performances of Ru(bpy)$_3^{2+}$ and EY, in two photoredox reactions.[35] The first reaction tested was the dehalogenation of α-haloacetophenones **5** (Scheme 5).[8] Here, EY outperformed the metal-based PC with better yields of the dehalogenated products **7** (Scheme 5, entries 1 *vs.* 2).

Importantly, when using EY, it was possible to use a less energetic 530 nm light which avoids the degradation of this photosensitiser while providing a clean and high yielding dehalogenation process. The authors also tested this organic PC in the photochemical asymmetric α-alkylation of aldehydes **8** (Scheme 6).[7] In this case, the use of 0.5 mol% of EY allowed the formation of the alkylated products **11** in comparable yields and enantioselectivities (Scheme 6a).

Following the working hypothesis of MacMillan,[7] the authors proposed the two cooperative catalytic cycles depicted in Scheme 6, where the EY orchestrates this process similarly to Ru(bpy)$_3^{2+}$ (Scheme 6a, entries 1 *vs.* 2). However, the highly different quantum yields obtained ($\varphi$ = 0.075 for EY *versus* $\varphi$ = 18 for Ru(bpy)$_3^{2+}$) revealed the operation of the two alternative mechanistic pathways.[36]

In the following work, Zeitler's group proved the possibility of merging EY with other activation modes, such as hydrogen-bonding catalysis. Specifically, the authors revisited the reductive cyclisation of (aryl)bisenones **12** under protic conditions, previously reported by Yoon's group with Ru(bpy)$_3^{2+}$.[37] In this case, the use of 20 mol% of thiourea **14** in combination with EY
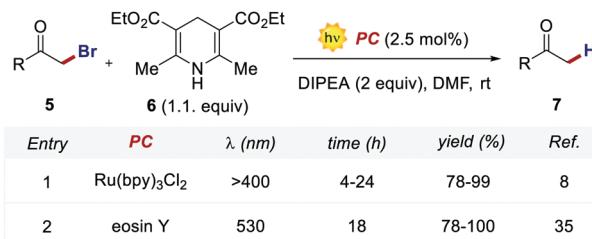


**Scheme 5** Photocatalytic reductive dehalogenation. Comparison between the performances of Ru(bpy)$_3^{2+}$ and eosin Y.
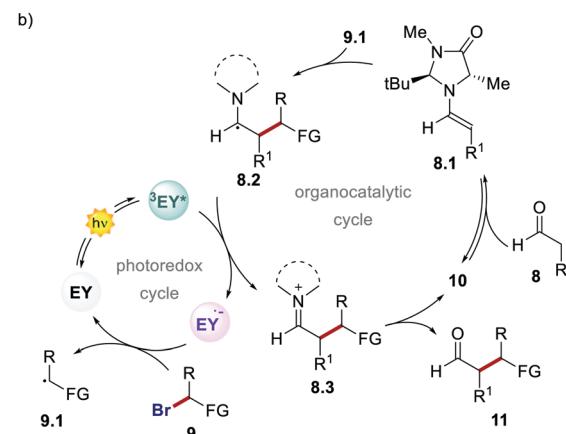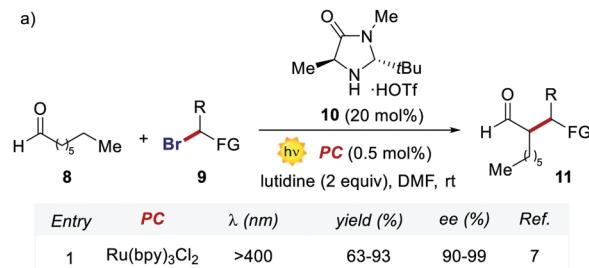


**Scheme 6** (a) Photo-organocatalytic enantioselective α-alkylation/perfluoroalkylation of aldehydes. Comparison between the performances of Ru(bpy)$_3^{2+}$ and eosin Y. (b) The proposed mechanism for the photochemical asymmetric α-alkylation of aldehydes with eosin Y.

afforded the cyclised products **13** with complete *trans*-diastereoselectivity, in comparable yields to the Ru-catalysed process (Scheme 7a, entries 1 *vs.* 2).[38]

Interestingly, the method implemented by Zeitler's group avoids the use of over-stoichiometric amounts of Lewis acids. Instead, this organocatalytic reaction relies on the ability of thiourea **14** to activate **12** through H-bond interactions (Scheme 7b), thus making the coordinated enone **12** more reactive towards the PET process with the EY•⁻. In this regard, the reductive power of the EY•⁻ ($E_{red}$ = −1.06 V *vs.* SCE in MeCN) proved to be sufficient to reduce a variety of enones **12**.

In 2013, Scaiano's group unveiled the potential of methylene blue **15** (MB) to serve as a purely organic PC (Scheme 8).[39] MB is characterised by a maximum absorption set at $\lambda$ = 650 nm (red-light), and a triplet state (³MB*) with a $\tau$ = 32 µs, which can participate in both oxidative and reductive quenching events.[40]

The use of this PC was previously limited to producing singlet oxygen for applications in the fields of chemistry and biology.[41]

In the work, Scaiano's group developed a metal-free variant of the photocatalytic oxidative hydroxylation of aryl boronic acids **16** with molecular oxygen (Scheme 9). Such transformation was previously reported by Xiao and Jørgensen's groups employing Ru(bpy)$_3^{2+}$ as a PC, but it suffered from prolonged reaction times (up to 72 h).[42] A direct comparison between Ru(bpy)$_3$Cl$_2$ and MB at a given reaction time (7 h) showed the superior performance of MB (Scheme 9a, entries 1 *vs.* 2).
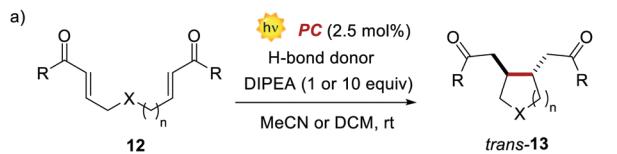
a)
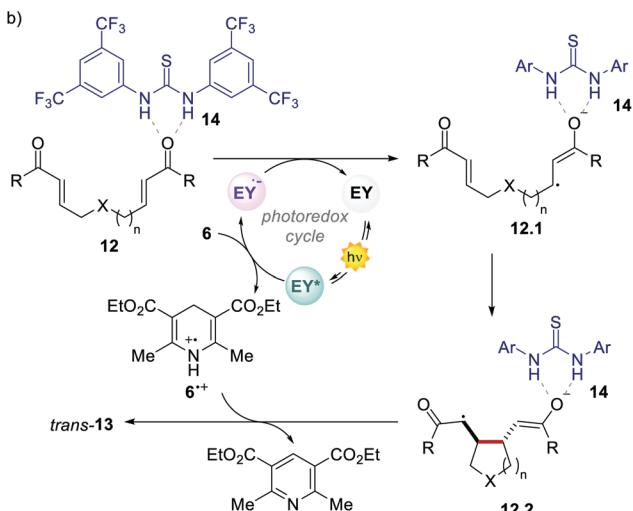


**Scheme 7** (a) Photo-reductive cyclisation of (bis)enones. Comparison between the performances of Ru(bpy)$_3^{2+}$ and eosin Y. (b) Mechanism of the reductive cyclisation of (aryl)bisenones promoted by eosin Y.
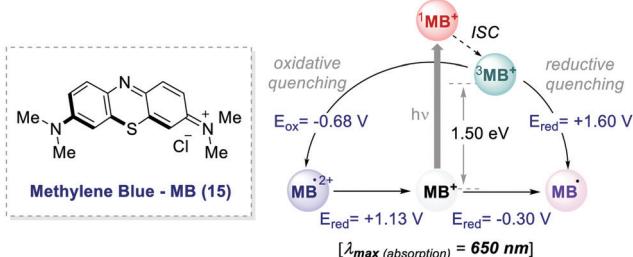


**Scheme 8** Photophysical properties and redox potentials (*vs.* SCE in MeCN) of methylene blue (ref. 40*c* and *d*).

The authors concluded that one of the key events in the photocatalytic cycle is the reductive quenching of the MB triplet state ($^3$MB$^+$) *via* a SET process from diisopropylethylamine (DIPEA **18**, Scheme 9b). In fact, kinetic investigations with laser flash photolysis revealed that $^3$MB$^+*$ is quenched nearly 40 times faster than Ru(bpy)$_3^{2+}*$.

Collectively, these reports emphasise the potential of already established organic dyes as suitable alternatives to transition metal chromophores and have encouraged the discovery of new families of versatile organic molecules serving as PCs. The search for new organic PCs capable to replace metal complexes is still an active research area. In this regard, one

a)
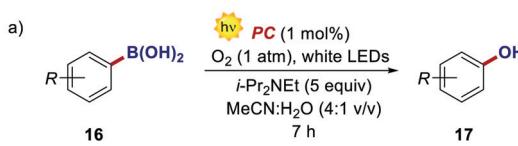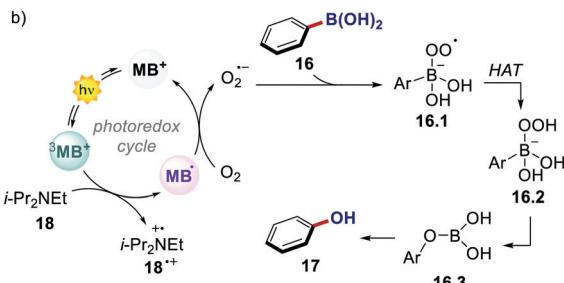


**Scheme 9** (a) Photocatalytic oxidative hydroxylation of aryl boronic acids. Comparison between the performances of Ru(bpy)$_3^{2+}$ and methylene blue. (b) Mechanistic proposal for the oxidative hydroxylation of aryl boronic acids with MB as PC.

of the latest examples has been documented by Gianetti's group.[43a] They have successfully applied *N*,*N*′-di-*n*-propyl-1,13-dimethoxyquinacridinium ($^n$Pr-DMQA$^+$) tetrafluoroborate salt **19** (Scheme 10) as an efficient PC in a variety of known photoredox reactions. This PC can be synthesized following a high-yielding multi-step procedure.[43b,c] One remarkable aspect of this PC is that it allows the use of red light ($\lambda$ = 600–700 nm), thus offering a milder option for the commonly used white, blue or even green light mediated photoreactions. Furthermore, this low-energy irradiation avoids side reactions, has fewer health risks and it is naturally abundant from sunlight.

The authors evaluated the performances of this new PC in the dual photoredox/Pd-catalysed C(sp$^2$)–H arylation of substituted arenes **20**, which was first documented by Sanford's group, using Ru(bpy)$_3^{2+}$ in the presence of a 26 W compact fluorescent light (CFL, Scheme 11).[44]

The replacement of Ru-PC for $^n$Pr-DMQA$^+$ provided enhanced results for the formation of the arylated product **22**, with the additional advantage of using low-energy red-light (entries 1 *vs.* 2, Scheme 11a). In the original light-driven process, the excited Ru(bpy)$_3^{2+}*$ reduces ArN$_2^+$ **21** to the aryl
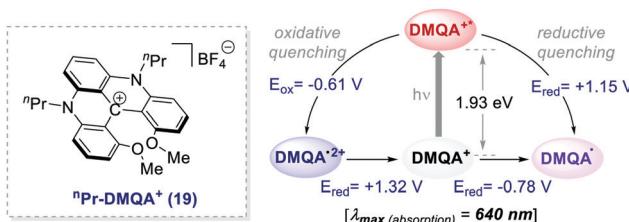


**Scheme 10** Photophysical properties and redox potentials (*vs.* SCE in MeCN) of $^n$Pr-DMQA$^+$ (ref. 43*a*).
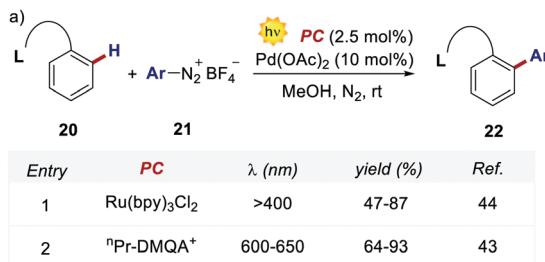
**Scheme 11** (a) Dual photoredox/Pd-catalysed C–H arylation of substituted arenes. Comparison between the performances of Ru(bpy)$_3^{2+}$ and $^n$Pr-DMQA$^+$. (b) The proposed mechanism for the photoredox/Pd-catalysed C–H arylation of arenes, depicted with DMQA+ as PC.



**Scheme 12** (a) Synthetic strategy for the assembly of the naphthochromenone scaffold. (b) Structures of the NTC photocatalysts (ref. 45).

radical **20.1** ($E^*_{ox}$ (Ru$^{III}$/Ru$^{II*}$) = −0.81 V; $E_{red}$ (PhN$_2^+$/Ph$^\bullet$) = −0.10 V *vs.* SCE in MeCN) (Scheme 11b). Then, the one-electron oxidation of the Pd$^{III}$-complex **20.2** by Ru(bpy)$_3^{3+}$ regenerates the Ru(bpy)$_3^{2+}$ ($E_{red}$ (Ru$^{III}$/Ru$^{II}$) = +1.29 V *vs.* SCE in MeCN). Following a similar mechanistic pathway, the excited DMQA$^{+*}$ undergoes an unconventional oxidative quenching with **21**, to deliver the required aryl radical **21.1** ($E^*_{ox}$ (DMQA$^{\bullet++}$/DMQA$^{+*}$) = −0.62 V *vs.* SCE in MeCN). The catalyst regeneration occurs through the reduction of DMQA$^{\bullet++}$ by the Pd-intermediate **20.2** ($E_{red}$ (DMQA$^{\bullet++}$/DMQA$^+$) = +1.32 V *vs.* SCE in MeCN). The photoinduced aerobic oxidative hydroxylation of arylboronic acids **16** (refer to Scheme 9) was also successfully promoted by DMQA$^+$ PC, using red-light irradiation. Under the new photochemical conditions, the benchmark product **17** (Scheme 9, with R = H) was obtained in 83% yield, thus outcompeting the performance of the Ru-complex PC (entry 1, Scheme 9a).

In 2020, Dell'Amico's group reported the synthesis, photophysical characterisation and use of naphthochromenones (NTCs), a novel class of bimodal PCs (Scheme 12).[45] The NTC scaffolds were assembled through a microfluidic photoenolization/Diels–Alder sequence from benzophenones,[46] followed by water elimination and aromatisation (Scheme 12a). This strategy allowed the synthesis of the six photoactive scaffolds **25a–f** (Scheme 12b). Further manipulation of **25e** provided another six additional structures (products **25g–l**).

The 12 NTCs absorb in the visible region towards the higher-energy region of the spectrum (400–420 nm). This feature allows the use of common LEDs for their excitation, but at the same time, guaranteeing access to a highly energetic excited

state (up to 3.22 eV). Additionally, their balanced and broad redox windows ($E^*_{red}$ up to 1.65 V, $E^*_{ox}$ up to −1.77 V *vs.* SCE in MeCN) make them able to engage in both reductive and oxidative quenching processes (Scheme 13).

The performances of the 12 NTCs were first evaluated in the Povarov-type addition of *N,N*-dimethylaniline **26** to phenylmaleimide **27** (Scheme 14). Interestingly, the methoxy-substituted NTC **25f** outperformed the previously reported yields achieved with Ru(bpy)$_3^{2+}$ and EY, which afforded product **28** in 83% and 82% yields, respectively (Scheme 14, entries 1 and 2 *vs.* 3). It is worth noting that the structurally simpler NTC **25a** provided the product in comparable yield to Ru(bpy)$_3^{2+}$ and EY (Scheme 14, entries 1 and 2 *vs.* 4).

Based on the reported mechanism,[47] the oxidation of aniline **26** occurs from the excited NTC*, generating the radical cation **26.1** ($E^*_{red}$ (**25f**/**25f**$^{\bullet-}$) = 1.21 V; $E_{ox}$ (**26**$^{\bullet+}$/**26**) = +0.80 V *vs.* SCE in MeCN). The resulting NTC **25f**$^{\bullet-}$ is then oxidised by O$_2$, thus closing the photoredox cycle ($E_{red}$ (**25f**/**25f**$^{\bullet-}$) = −1.76 V; $E_{red}$ (O$_2$/O$_2^{\bullet-}$) = −0.64 V *vs.* SCE in MeCN). The formation of the product occurs through the addition of the α-aminoradical **26.2**
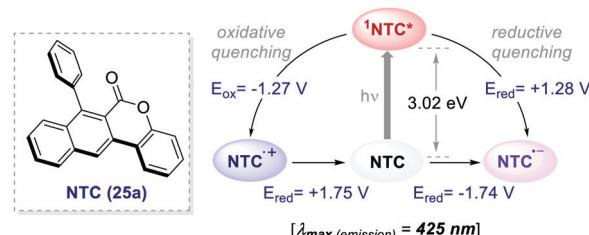


**Scheme 13** Photophysical properties and redox potentials (*vs.* SCE in MeCN) of NTC 25a (ref. 45).

a)



| Entry | PC | λ (nm) | yield (%) | Ref. |
|-------|-----|--------|-----------|------|
| 1 | Ru(bpy)₃Cl₂ | 400–420 | 83 | 47a |
| 2 | eosin Y | 530 | 82 | 47b |
| 3 | NTC **25f** | 400 | 89 | 45 |
| 4 | NTC **25a** | 400 | 78 | 45 |

b)
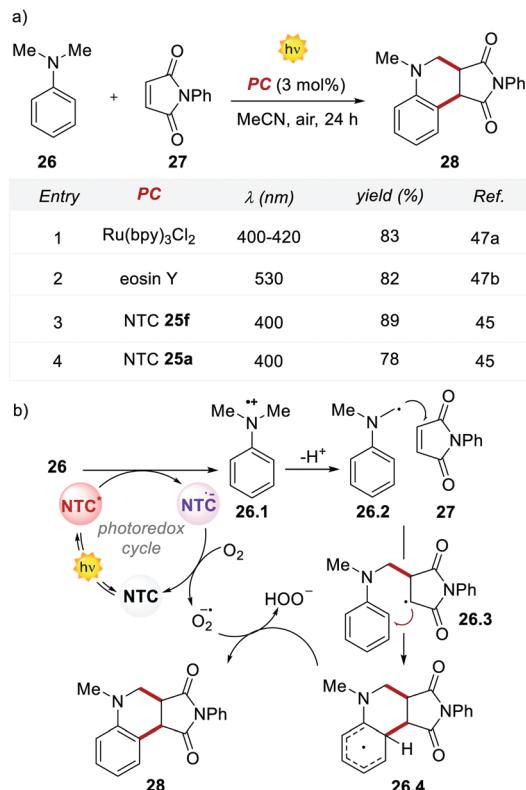


**Scheme 14** (a) Povarov-type addition of *N,N*-dimethylaniline to phenylmaleimide. Comparison between the performance of Ru(bpy)₃²⁺ and NTC **25f**. (b) The reported mechanism for the Povarov-type addition of *N,N*-dimethylaniline to phenylmaleimide, depicted with NTCs as PCs.

to **27**, leading to **26.3**. A second radical cyclization event, followed by the oxidation of the resulting intermediate **26.4**, delivers product **28**.

### 4.2 Replacement of an Ir-complex for an organic PC

Ir-based PCs have also found extensive use in photoredox catalysis. The complex *fac*-Ir(ppy)₃ **2a** absorbs visible photons ($\lambda_{max}$ = 375 nm), giving access to a long-lived triplet ³MLCT state ($\tau$ = 1.9 μs).[14] It is a strong reductant in the excited state ($E^*_{ox}$ = −1.79 V *vs.* SCE in MeCN), and a relatively poor oxidant ($E^*_{red}$ = 0.31 V *vs.* SCE in MeCN) (Scheme 15).

Research towards the identification of suitable organic alternatives to this strongly reducing Ir complex initially began in the field of polymer chemistry, specifically in atom transfer
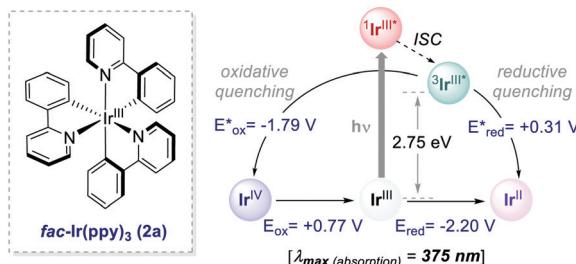


**Scheme 15** Photophysical properties and redox potentials (*vs.* SCE in MeCN) of *fac*-Ir(ppy)₃ (ref. 14).

radical polymerisation (ATRP). Controlled radical polymerisations (including ATRP) are synthetic processes that allow obtaining polymers with low dispersity, precise molecular weight and controlled composition.[48]

The use of purely organic PCs in polymerisation reactions is essential because the metal-traces contamination in a polymeric material prevents any possible applications.[49]

In 2011, Choi's group presented the first method of photo-induced radical polymerisation of methyl methacrylate **30**.[50] In 2012, Hawker's group proposed the first visible light controlled ATRP of **30** with *fac*-Ir(ppy)₃, which allowed an improved control on the chain growth.[51] The PC operates through an oxidative quenching mechanism with the growing polymer chain (Scheme 16). The continuous activation and deactivation of the chain limit the number of active radicals present at the same time in the system. This mechanism also results in superior control over molecular weight dispersity.

Consequently, the main challenge for replacing the *fac*-Ir(ppy)₃ with an organic PC is to develop a strong photo-reductant with appropriate redox potentials to promote the reduction of the alkyl halide, while maintaining the ideal equilibrium between the activation and deactivation events (Scheme 16).

The earliest examples of photoinduced organic ATRP (O-ATRP) dates back to 2014, when Hawker's and Miyake's groups independently reported a metal-free method for the polymerisation of **30**.[52] Hawker successfully proposed the use of 10-phenyl phenothiazine **31** (PTH) as an organic PC (Scheme 17), whereas Miyake employed perylene. PTH was synthesized by the authors from commercially available phenothiazine and chlorobenzene in a one-step procedure through routine C–N cross-coupling reactions.

In both cases, the PCs operate through an oxidative quenching mechanism. They showed excellent results in terms of dispersion and retention of the chain end functionality.

PTH gave also access to the polymerisation of monomers that were inaccessible with Ir-based PCs. The polymerisation of dimethylaminoethyl methacrylate **32** was reported (Scheme 18) following the same oxidative quenching mechanism. PTH
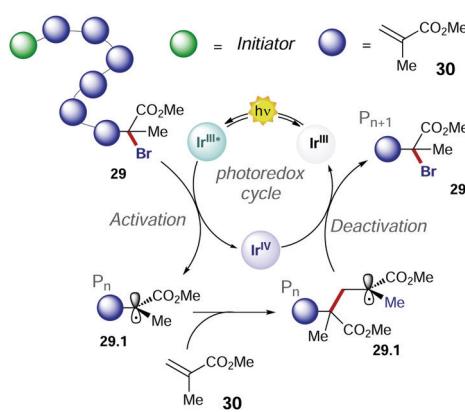


**Scheme 16** Mechanism of polymerisation of methyl methacrylate with *fac*-Ir(ppy)₃.
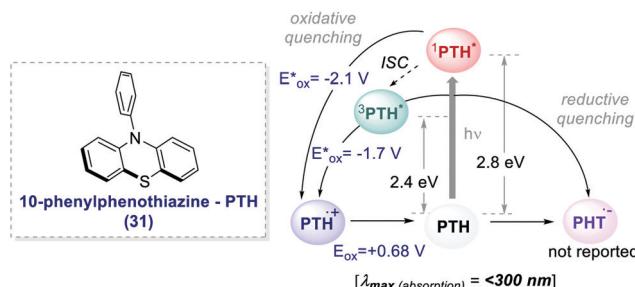
**Scheme 17** Photophysical properties and redox potentials (*vs.* SCE in MeCN) of PTH (ref. 25*c*).

achieved a much lower level of dispersion in comparison with *fac*-Ir(ppy)$_3$, showing a better control on the growth of the chain (Scheme 18a, entry 1 *vs.* entry 2).

The authors suggested that the reason was the difference in the $E_{ox}$ of PTH and *fac*-Ir(ppy)$_3$, respectively +0.68 V and +0.77 V *vs.* SCE in MeCN. The higher ground-state oxidation potential of *fac*-Ir(ppy)$_3$ causes the oxidation of the amino group of the monomer, and this decreases the control over the growth of the polymer chain.

Shortly after, these highly reducing organic dyes started to find applications as photocatalysts for small molecule activation. In 2015, Hawker's group, inspired by the results of O-ATRP, proposed the use of PTH as a replacement for *fac*-Ir(ppy)$_3$ in the dehalogenation of alkyl halides, following the report by Stephenson with *fac*-Ir(ppy)$_3$.[53,54] Employing PTH, the authors extended the application of this protocol not only to aryl iodides but also to difficult-to-activate substrates such as aryl bromides and chlorides (Scheme 19a). PTH was used in higher loading than *fac*-Ir(ppy)$_3$. However, the authors pointed out that 1 mg of PTH is more than 7000 times cheaper than 1 mg of *fac*-Ir(ppy)$_3$. The reaction mechanism, originally proposed by Stephenson, begins with the reduction of aryl halide **34** and the subsequent

| Entry | X | PC | mol % | time (h) | Condition | yield (%) | Ref. |
|-------|---|-----|-------|----------|-----------|-----------|------|
| 1 | Br | *fac*-Ir(ppy)$_3$ | 1 | 72 | inert atm. | 0 | 54 |
| 2 | Br | PTH | 5 | 72 | inert atm. | 85 | 53 |
| 3 | I | *fac*-Ir(ppy)$_3$ | 1 | 1 | inert atm. | 23 | 54 |
| 4 | I | PTH | 5 | 1 | inert atm. | 98 | 53 |
| 5 | I | *fac*-Ir(ppy)$_3$ | 1 | 2 | open air | 0 | 54 |
| 6 | I | PTH | 5 | 2 | open air | 57 | 53 |

**Scheme 19** (a) Reductive dehalogenation of aryl halides. Comparison between the performances of PTH and *fac*-Ir(ppy)$_3$. (b) Mechanism of the dehalogenation reaction. (c) Graphical depiction of the reduction potentials (*vs.* SCE in MeCN) of the selected aryl halides and $E_{ox}^*$ of PTH and *fac*-Ir(ppy)$_3$.

formation of the radical **34.1** upon the homolytic cleavage of the carbon–halogen bond. Product **35** is finally obtained after a H-atom abstraction event. The oxidation of tributyl amine **36** closes the photocatalytic cycle restoring the ground-state PC. Dehalogenation of phenyl bromide **34b** performed with PTH resulted in 85% yield in 72 hours while no conversion was observed with *fac*-Ir(ppy)$_3$. This result is a consequence of the higher $E_{ox}^*$ of the organic photocatalyst. Contrary to *fac*-Ir(ppy)$_3$, with PTH, both the $S_1$ and $T_1$ states can take part in the reduction of the carbon–halogen bond.

Despite the fact that the $S_1$ state is dominant due to its longer lifetime, the reduction of unactivated aryl bromides or chlorides is achieved only by the more reducing $S_1$ state. This feature was confirmed by carrying out a control reaction open to air in the presence of oxygen, which is a well-known triplet quencher.[55] The tolerance to oxygen was tested with different substrates and in every case, no reaction was observed with iridium. PTH was tested also in a higher-scale reaction

| Entry | PC | mol % | Đ |
|-------|-----|-------|---|
| 1 | *fac*-Ir(ppy)$_3$ | 0.005 | 3.69 |
| 2 | PTH | 0.1 | 1.11 |

**Scheme 18** (a) Polymerisation of dimethylaminoethyl methyl methacrylate. Comparison between the performances of PTH and *fac*-Ir(ppy)$_3$. (b) Graphical depiction of the oxidation potentials (*vs.* SCE in MeCN) of **32**, PTH and *fac*-Ir(ppy)$_3$.

with excellent results. Notably, during the purification of the product, PTH was also isolated and reused with unvaried reactivity.

In 2020, Dell'Amico's group chose this dehalogenation reaction to evaluate the performances of NTCs under oxidative quenching.[45] Thus, following the same mechanistic scheme, the reduction of methyl 4-iodobenzoate **37** was examined (Scheme 19). Interestingly, NTC **25a** performed well, achieving the formation of **34** in 86% yield. The more reducing NTC **25i** delivered **38** in 96% yield, providing a valuable metal-free alternative to *fac*-Ir(ppy)₃.[54] It is worth noting how NTC **25a** could be successfully employed under both oxidative (Scheme 20) and reductive quenching (Scheme 14), thus being a competent metal-free alternative to both Ru(bpy)₃²⁺ and *fac*-Ir(ppy)₃.[45]

In 2017, Ooi's group proposed the use of 3,6-dimethoxy-9*H*-thioxanthen-9-one **39** (TX, Scheme 21), a fully organic PC synthesized in three steps and high overall yield, to replace *fac*-Ir(ppy)₃ for the light-promoted imidation of arenes (Scheme 22).[56,57] The mechanism proceeds *via* the generation of the nitrogen-centred radical **40.1** upon the oxidative quenching of the PC* by the redox-active ester **41**, and the subsequent formation of radical **41.1** (Scheme 22b). The Wheland intermediate **41.2** is then formed upon the reoxidation of **41.1** by PC•⁺.

Ooi's group replaced *fac*-Ir(ppy)₃ with TX **39** and the reaction was optimised with the redox-active ester **40b**. The organic PC outperformed *fac*-Ir(ppy)₃ with various substrates including caffeine.

With appropriate substituents, Ir-based PCs can also operate under reductive quenching mechanisms. In 2014, McMillan's

Scheme 22 (a) Light-promoted imidation of arenes. Comparison between the performances of TX and *fac*-Ir(ppy)₃. (b) Mechanism of the light-promoted imidation of arenes.

group reported the use of the iridium complex **2d** (Scheme 23) as the photooxidant in a decarboxylative Giese-type radical addition (Scheme 24a, entry 4).[58]

This challenging reaction was used also by Dell'Amico's group to further evaluate the performance of NTCs under reductive quenching. The mechanism depicted in Scheme 24b follows a reductive quenching mechanism. The first step is the oxidation of **43** by the excited photocatalyst and the subsequent formation of the α-amino radical **43.1**. This reacts with the electron-poor olefin **44** generating the radical intermediate **43.2** which is then reduced by PC•⁻ closing the photoredox cycle. NTC **25a** gave a yield of 66% but the best result was delivered by NTC **25j** with a yield of 77% (Scheme 24a, entries 1 and 2).

Scheme 20 Reductive dehalogenation of methyl 4-iodobenzoate. Comparison between the performances of NTCs and *fac*-Ir(ppy)₃.
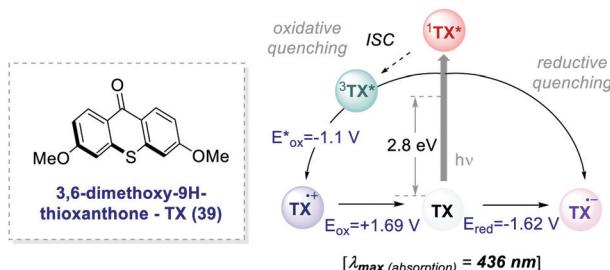
Scheme 21 Photophysical properties and redox potentials (*vs.* SCE in MeCN) of TX (ref. 25c).
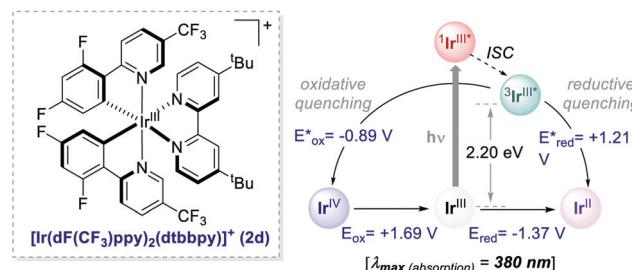
Scheme 23 Photophysical properties and redox potentials (in MeCN) of [Ir[dF(CF₃)ppy]₂(dtbbpy)]⁺ (ref. 15).
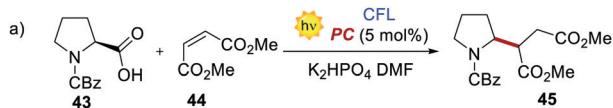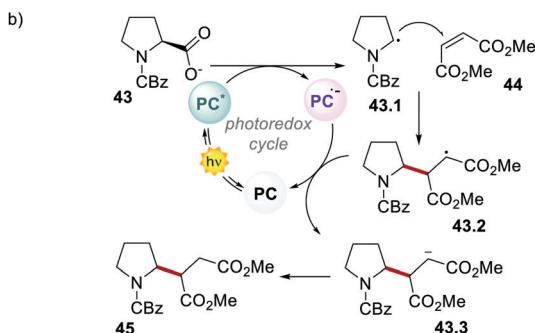
**Scheme 24** (a) Decarboxylative Giese-type addition of **43** and dimethyl maleate **44**. Comparison between the performances of NTCs and Ir-based PCs. (b) Mechanism of the decarboxylative Giese-type addition.

Conversely, *fac*-Ir(ppy)$_3$ was ineffective in this reaction (Scheme 24a, entry 3).

Despite the fact that NTCs performed slightly worse than **2d**, it is relevant to notice that NTC **25a** was applied successfully in various photochemical transformations under both oxidative and reductive quenching (Schemes 14, 20 and 24).[45]

# 5 Pushing the boundaries of photoredox catalysis with organic PCs

As mentioned, organic PCs are not only cheaper and sustainable alternatives to metal complexes, but they have also allowed the activation of previously unreactive targets, exceeding the redox limits of their metal counterparts. This significant feature has allowed the discovery of unprecedented reactivity and the development of previously inaccessible chemical transformations. In this section, we highlight that privileged organic PCs can perform thermodynamically demanding photoredox cycles.

## 5.1 Highly oxidising organic PCs

One of the most used highly oxidising PC classes is acridinium salts (**46a–c**, Scheme 25). Their scaffold was introduced by Fukuzumi in 2001,[59] and later was widely used and modified by Nicewicz among others.[60] The ground-state reduction of acridinium ions occurs at moderate potentials (around −0.5 V *vs.* SCE). In contrast, their excited state is characterised by a very high oxidative power, reaching redox potentials [$E_{red}$ (Acr$^{+}$*/Acr$^{•}$)] up to +2.32 eV. Structural modifications of the acridinium core have allowed improving their chemical
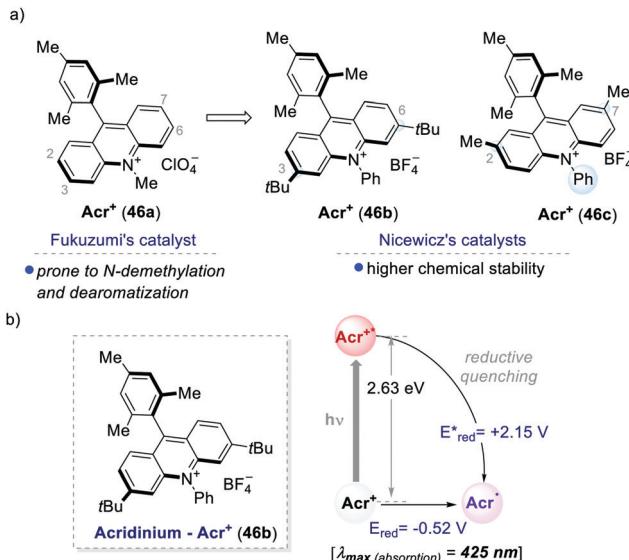


**Scheme 25** (a) Representative acridinium catalysts developed by Fukuzumi's and Nicewicz's groups. (b) Photophysical properties and redox potentials (in MeCN) of Acr$^{+}$ **46b** (ref. 25c).

stability towards (i) *N*-dealkylation reactions and (ii) nucleophilic or radical additions at the 2,7 or 3,6-positions.[26a]

Acridinium ions, synthesized through multi-step procedures,[60] have been efficiently used as PCs under reductive quenching for a wide variety of thermodynamically challenging redox processes, including the oxidation of alkenes.[61,62] In this regard, Nicewicz's group has reported various photochemical methods for the intra- and intermolecular anti-Markovnikov addition of different heteronucleophiles, using Acr$^{+}$ **46a** and a redox active hydrogen atom donor (Scheme 26a).[60a,63] The general postulated mechanism for these transformations involves the initial formation of the alkene radical cation **49.1** by single-electron oxidation (Scheme 26b, inter-molecular manifold shown), followed by nucleophilic addition with a nucleophile (*Nu* in Scheme 26b) with anti-Markovnikov regioselectivity. The desired hydro-functionalised product **50** is then formed after a hydrogen atom transfer (HAT) event. Regeneration of the catalyst Acr$^{+}$ **46a** occurs by another SET process between the thiyl radical **51.1** and the acridinium radical Acr$^{•}$ **46a**. Considering the reduction potentials of this substrate couple ($E_{red}$ (**46.1/46.2**) = +0.45 V *vs.* SCE[64] and $E_{ox}$ (Acr$^{+}$ **46a**/Acr$^{•}$ **46a**) = −0.57 V *vs.* SCE[59,65]), this latter step is thermodynamically favoured. Notably, this photochemical method allows the use of alkenes having oxidation potentials up to 2.10 V. Such values are well beyond the redox potentials of the common Ir- and Ru-based PCs.

In the following studies, Nicewicz's group has showcased the potential of acridinium PCs to provide new metal-free strategies for the C–H functionalisation of arenes.[66] In 2015, they used the more robust catalyst Acr$^{+}$ **46b** ($E^{*}_{red}$ = +2.25 V) to develop a site-selective C–H amination of substituted aromatic compounds (Scheme 27a).[60b] This transformation exploits the ability of the photoexcited acridinium Acr$^{+}$* **46b** to generate arene radical cations **47.1** through a single electron oxidation
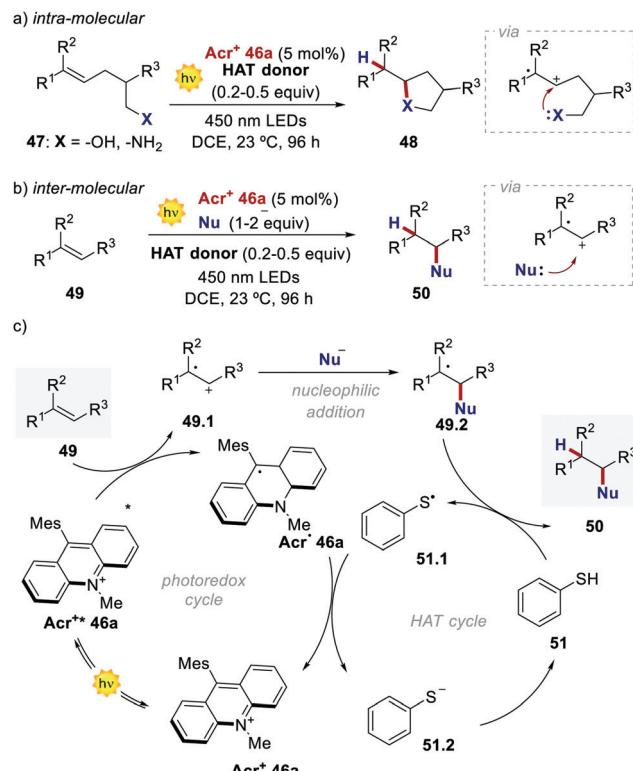
Scheme 26 (a) Catalytic intra- and inter-molecular anti-Markonikov hydrofunctionalisation of alkenes enabled by the photocatalytic activity of acridinium salts. (b) General mechanism (for simplicity, only the inter-molecular reactivity is shown). **Nu**: nucleophile. **HAT**: hydrogen atom transfer.



Scheme 27 (a) Photochemical C–H amination of arenes enabled by acridinium PCs. (b) One of the plausible mechanisms [ref. 60b].

pathway (Scheme 27b). Then, the nucleophilic addition of amine **53** on the intermediate **52.1**, followed by the oxidation of the resulting species **52.3**, delivers the C–N-coupled arene adduct in high yields (up to 88%) and with good to excellent levels of regioselectivity (up to >20:1). During the optimization studies, degradation of the acridinium catalyst was observed, as well as of the starting arene derivative **52** (where R[1] = –OMe). Indeed, both compounds are prone to decompose in the presence of oxygen-centred radicals that may be formed during the reaction, under the presence of O$_2$.[60c] Such a degradation pathway was mitigated by the addition of 20 mol% of TEMPO **55**, thus improving the yield of the process.

Recently, new libraries of acridinium salts with diverse photophysical and electrochemical properties were reported, facilitating a rational selection of the most adequate acridinium PC for a given photoredox transformation.[67] Interestingly, Sparr's group has recently documented three protocols for the synthesis of libraries of symmetrical 3,6-diamino- and 1,8-dimethoxy-substituted PCs (**56** and **57**, respectively, in Scheme 28a), as well as unsymmetrical acridiniums (**58**).[67a,b,f]

Interestingly, the performance of some of these new PCs was tested in various photoreactions, showing comparable or even enhanced results relative to the ones offered by the corresponding Ir- or Ru-PCs. For instance, acridiniums **56** exhibited redox potentials similar to those of iridium complex



Scheme 28 (a) Emerging acridinium libraries. (b) Comparison of the performances between an acridinium derivative **56** and an Ir–PC, in a photoredox-Ni catalysed decarboxylative cross-coupling process.

**2d** ($E_{red}$ (Ir$^{III}$/Ir$^{II}$) = −1.37 V; $E_{red}$ (Ir$^{III}$*/Ir$^{II}$) = +1.21 V vs. SCE).[67a] This feature allowed the use of these new PCs in the metallaphotoredox-nickel catalysed decarboxylative cross-coupling between aminoacids **59** and aryl halides **60** (Scheme 28b). This photochemical process was originally developed by MacMillan and co-workers in 2014, using **2d** as the optimal PC.[68] In Sparr's work, the mesityl-substituted
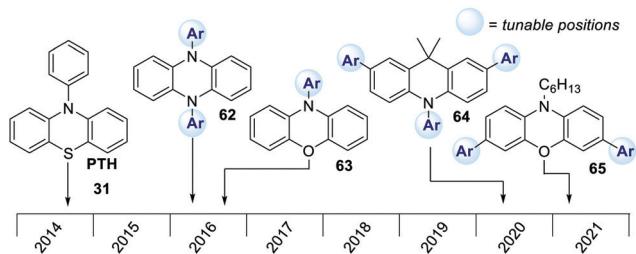
Scheme 29 Main classes of organic PCs employed in O-ATRP.



Scheme 30 Photophysical properties and redox potentials (*vs.* SCE, in MeCN) of POx (ref. 25*d*).

catalyst **56** (where Ar = 2,4,6-trimethylphenyl) could promote the same transformation with very similar results (86% yield with **56** *vs.* 90% yield with **2d**), thus highlighting the potential of these new families of PCs for replacing their metal counterparts.

## 5.2 Highly reducing organic PCs

In the last few years, research on strongly reducing organic PCs has rapidly evolved. Many new PCs were introduced to replace metal complexes. Also, in this case, most of them were first applied in O-ATRP. In 2016, Miyake's group reported the synthesis and use of 5,10-dihydrophenazines **62** and *N*-aryl phenoxazine **63**. More recently, the same group reported the successful use of dihydroacridines **64** and *N*-alkyl phenoxazines **65** (Scheme 29).[69]

Despite their similar structures, PC **63** displayed enhanced abilities in the O-ATRP of methyl methacrylate **30** in comparison with PTH. Due to the bigger size of the sulfur atom, PTH adopts a bent conformation in the ground state, whereas PC **63** is planar. Nevertheless, they both assume a planar conformation in the excited state. Consequently, the former has a higher reorganisation energy that decreases the rate of electron transfer during the reduction of PTH•+ to restore the ground-state PTH. In 2018, Miyake's group performed structure–property relationship studies on phenoxazine-based photocatalysts.[26b] This study was made possible by the high synthetic versatility and availability phenoxazine scaffold. C–N coupling was exploited to functionalize the nitrogen atom. The functionalization of the main core was accomplished in a two-step process: (i) radical bromination, followed by (ii) a cross-coupling reaction.

Different substituents in the core of the molecule and on the *N*-aryl moiety can dramatically alter the redox potentials and the absorption spectrum. The result was the generation of a library of 19 different PCs whose triplet $E_{ox}^*$ covers a wide window ranging from −2.11 to −1.40 V *vs.* SCE.

One of the most promising candidates is 3,7-4(biphenyl)-1-naphthalene-10-phenoxazine **66** (POx) represented in Scheme 30.

The addition of biphenyl substituents at positions 3 and 7 of the phenoxazine core doubles the molar absorptivity and redshifts the maximum wavelength of absorption by 65 nm compared to the unsubstituted counterpart. Therefore, the absorption profile reaches the visible region, contrary to PC **63**. The naphthyl moiety on the nitrogen atom instead allows the access to a CT excited state from the electron-rich core.[26b]
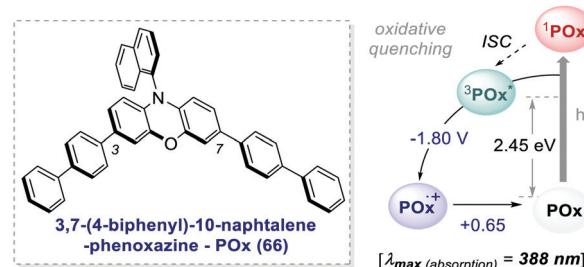
The capability to work under visible-light and the exceptionally long triplet lifetime of 480 μs[25d] made this PC suitable for various photochemical reactions.

In 2018, König's group used **66** in a Barbier-type reaction for the allylation of aldehydes and ketones (Scheme 31).[70] The mechanism (Scheme 31b) follows an oxidative quenching cycle and involves the reduction of benzaldehyde **67** with the formation of a ketyl radical **67.1**. Remarkably, product **69a** is obtained in higher yields and with less formation of the homocoupling side products **69b** and **69c**, by using POx **66** instead of the Ir catalyst **2d**.

POx **66** was used also by Jui's group in 2019 for the functionalisation of the C–F bond of unactivated trifluoromethyl arenes.[71] At temperatures higher than 50 °C, POx performed better than *fac*-Ir(ppy)₃ and PTH (Scheme 32a). The higher conversion achieved was a result of the longer excited state lifetime of POx compared to the other PCs.
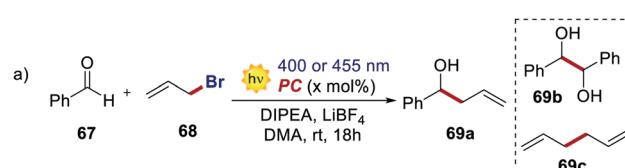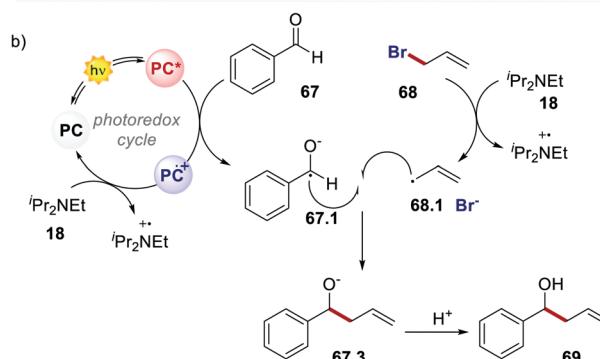


Scheme 31 (a) Barbier-type reaction between benzaldehyde and allyl bromide. Comparison between the performances of POx and [Ir(dF(CF₃)ppy)₂(dtbbpy)]⁺. (b) Mechanism of the Barbier-type reaction.

a)



| Entry | PC | mol % | yield (%) |
|---|---|---|---|
| 1 | POx | 2 | 86 |
| 2 | PTH | 10 | 48 |
| 3 | *fac*-Ir(ppy)₃ | 2 | 64 |

b)
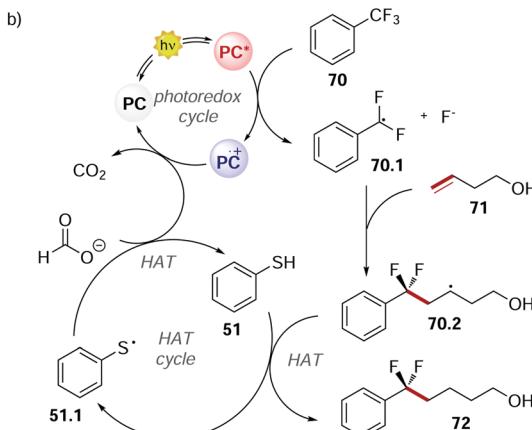


**Scheme 32** (a) Selective C–F functionalisation of unactivated trifluoro-methyl arenes. Comparison between the performances of POx, PTH and *fac*-Ir(ppy)₃. (b) Mechanism of the C–F functionalisation.

a)



| Entry | PC | $\lambda$ (nm) | yield (%) | Ref. |
|---|---|---|---|---|
| 1 | NTC **25j** | 400 nm | 88 | 45 |
| 2 | NTC **25a** | 400 nm | 69 | 45 |
| 3 | Ru(bpy)₃Cl₂ | 400 nm | - | 45 |
| 4 | *fac*-Ir(ppy)₃ | 400 nm | - | 45 |
| 5 | TBADT | 310 nm | 60 | 73 |

b)
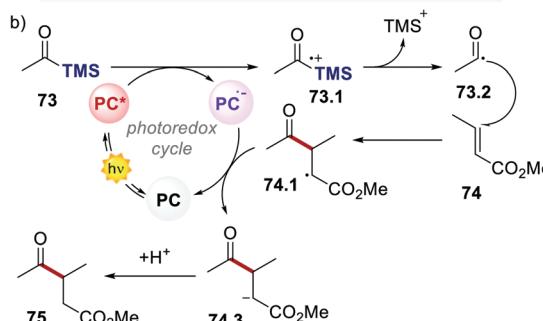


**Scheme 33** (a) Light-driven Giese-type acylation of methyl crotonate. Comparison between the performances of various PCs. (b) The proposed mechanism for the light-driven acylation of methyl crotonate.

This mechanism (Scheme 32b) is an example of dual photocatalysis where a photoredox cycle is merged with a second catalytic cycle with a different activation mode.[72]

The excited PC reduces **70** and, upon the cleavage of the C–F bond, radical **70.1** is formed. This radical undergoes intermolecular addiction with olefin **71**. Finally, a HAT event between the alkyl radical **70.2** and thiophenol **51** provides product **72**. Potassium formate is needed in stoichiometric amounts to close both the photoredox cycle and the HAT cycle restoring the PC and **51**, liberating CO₂ as a traceless side product.

### 5.3 Bimodal organic PCs

**5.3.1 Naphthochromenones.** The NTCs reported by Dell'Amico proved competent in promoting organic transformations that classically make use of Ru and Ir complexes. The broader redox potentials of NTCs rendered them able to outperform Ru and Ir PCs in diverse synthetically relevant transformations.[45]

The light-driven acylation of methyl crotonate **74** by acetyl silane **73** was performed using the developed NTCs (Scheme 33). According to the reported reaction mechanism, the PC needs to exceed an $E_{red}^*$ of 1.46 V to engage in reductive quenching with acetyl silane **73**.[73] Giese-type addition of **73.2** to methyl crotonate **74** yields the intermediate **74.1**, which is reduced by PC•⁻. In this step, the thermodynamic requirement is that the $E_{ox} < -0.6$ V.[74] NTC **25j** ($E_{red}^* = 1.56$ V and $E_{ox} = 1.45$ V) delivered the product in 88% yield. The simpler NTC **25a** also provided the product in synthetically useful yield. Importantly,

under the same experimental conditions, product **75** was not obtained using Ru(bpy)₃²⁺ or *fac*-Ir(ppy)₃.

The reductive dehalogenation of 4-cyanobenzyl halides **76** was also investigated with NTCs to benchmark their performances in an oxidative quenching cycle (Scheme 34). When using NTC **25k**, product **77** was obtained in 51% yield. The use of highly reducing *fac*-Ir(ppy)₃ only led to traces of the desired product, while *fac*-Ir(dFppy)₃ gave the product in only 19% yield. Ru(bpy)₃²⁺ was not a competent catalyst for the transformation, and no product was detected.

**5.3.2 Cyanoarenes.** Cyanoarenes are a class of photoactive molecules with an aromatic core bearing at least one cyano moiety. The most popular PC of this class is 1,2,3,5-tetrakis(carbazol-9-yl)-4,6-dicyanobenzene **78** (4CzIPN). First reported by Adachi in 2012 to be used in OLEDs,[75] its structure
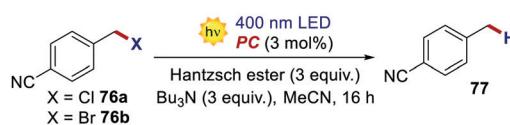


| Entry | PC | yield (%), X = Cl |
|---|---|---|
| 1 | NTC **25k** | 54 |
| 2 | Ru(bpy)₃Cl₂ | - |
| 3 | *fac*-Ir(ppy)₃ | < 5 |
| 4 | *fac*-Ir(dFppy)₃ **2b** | 19 |

**Scheme 34** Light-driven reduction of 4-cyanobenzyl halides. Comparison between the performances of various PCs.
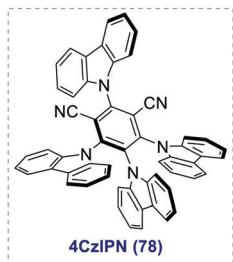
**Scheme 35** Photophysical properties and redox potentials (*vs.* SCE, in MeCN) of 4CzIPN (ref. 26*c*).

was designed in order to have a small energy gap between the $S_1$ and $T_1$ states. This feature allows reverse intersystem crossing (RISC) from $T_1$ to $S_1$ at room temperature. 4CzIPN thus exhibits thermally activated delayed fluorescence (TADF) with a remarkably long lifetime in the timescale of μs. Its strong CT character in the excited states also contributes to the long lifetime. Its balanced redox potentials make it a versatile bimodal PC (Scheme 35).

In 2016, Zhang and Luo reported the first synthetic use of 4CzIPN in a dual photoredox/Ni cross-coupling as a cost-effective alternative to iridium complex **2d**.[76] In 2018, Zeitler's group expanded the class of cyanoarenes derived from isophthalonitrile (IPN) and benzonitrile (BN), showing how the rational design of photocatalytic scaffolds can deliver PCs able to engage in both oxidative and reductive quenching cycles.[26c]

The redox potentials of the prototypical 4CzIPN are close to those of iridium complex **2d**, and 4CzIPN is often used as its metal-free alternative. It is however worth pointing out the main advantage of cyanoarenes. In 4CzIPN and its analogues, the HOMO and LUMO are spatially separated on the donor substituents and the acceptor core, respectively. Hence, it is possible to build a wide library of PCs with fine-tailored redox potentials in straightforward single-step syntheses (Fig. 6).[26c,76] The evaluation of the thermodynamic requirements of each reaction guides the rational selection of the *ad hoc* derivative.

The molecular structure of 4CzIPN is essential to its success in a recent example of dual photoredox/HAT catalysis. In 2019, König's group reported the redox-neutral photocarboxylation of benzylic C–H bonds (Scheme 36).[77] During the initial screening of the PCs, 4CzIPN provided product **79** in 14% yield, while *fac*-Ir(ppy)₃ and iridium complexes **2c** and **2d** were completely ineffective. Further optimisation with 4CzIPN increased the yield to 57%. Under reaction conditions, 4CzIPN is converted into its benzylated derivative 3CzPEBN. Its radical anion 3CzPEBN•⁻ ($E_{red} = -1.69$ V for 3CzPEBN) is a much stronger reductant compared to 4CzIPN•⁻ ($E_{red} = -1.24$ V for 4CzIPN) and is thus able to reduce the benzylic radical **79.1** ($E_{red} = -1.60$ V *vs.* SCE) to the anion **79.2**. 3CzPEBN is the active catalyst in the transformation, which also explains the lack of reactivity observed with the Ir-based PCs.

Very recently, Dell'Amico, Magnier and Togni's groups reported a protocol for the radical α-trifluoromethoxylation of ketones under photoredox conditions (Scheme 37).[78] The selection
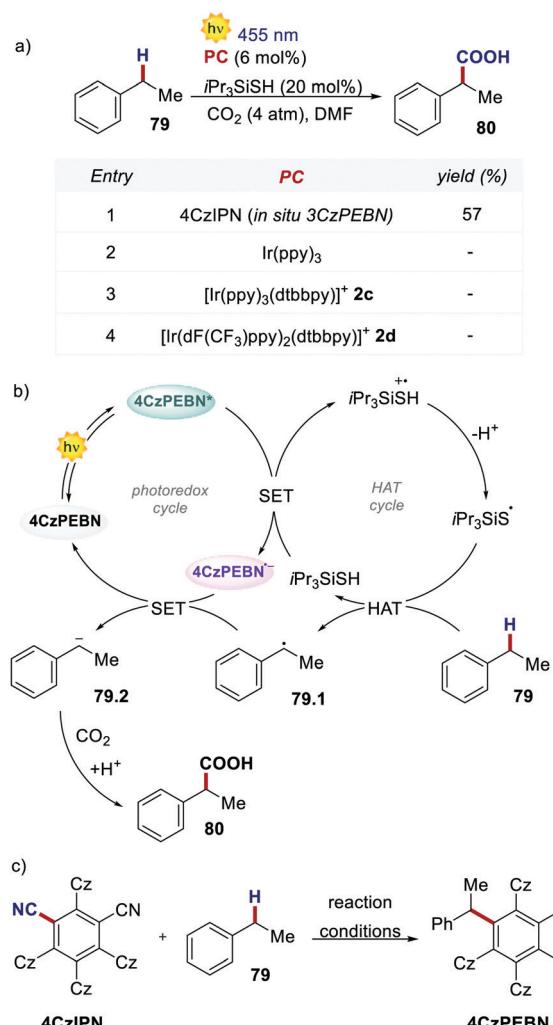


**Scheme 36** (a) Dual photoredox/HAT catalysis for the carboxylation of C–H benzylic bonds. Comparison between the performances of various PCs. (b) Proposed reaction mechanism for the carboxylation of C–H benzylic bonds. (c) *In situ* formation of 3CzPEBN.



**Fig. 6** Common acceptor and donor moieties for cyanoarenes synthesis.

**Scheme 37** Radical α-trifluoromethoxylation of ketones.

of an organic PC was key for increasing the regioselectivity of the reaction. During the optimisation, the use of Ru(bpy)$_3$$^{2+}$ afforded a regioselectivity of 12:1 between **83a** and **83b**, with significant trifluoromethoxylation on the aromatic ring.[79] With NTC **25a**, the ratio was improved to 13:1, albeit with a lower reactivity. When using 4CzIPN, the trifluoromethoxylation took place with full selectivity on the alpha position of the ketone (3:4 ratio >20:1) and with increased yield.

# 6 Consecutive photoinduced electron transfer: overcoming the thermodynamic limits in photoredox catalysis

According to the Rehm–Weller theory, the excited state energy $E_{0,0}$ of a PC sets the maximum redox potential window achievable under oxidative or reductive quenching.[4] For a PC absorbing in the visible region (>400 nm), the maximum $E_{0,0}$ approaches 3 eV. However, energy losses due to ISC or non-radiative processes further decrease this value. This issue poses a lower thermodynamic limit for PET and for several synthetically valuable transformations that can be carried out.

Consecutive photoinduced electron transfer (ConPET) is a catalytic solution to this limitation, first reported by König's group in 2014 using perylene diimide (PDI) as an organic PC.[80] Through a ConPET, it is possible to overcome the thermodynamic limitations of PCs by expanding their redox borders.

The general concept of ConPET involves (i) the PC excitation and (ii) the subsequent quenching by a suitable donor or acceptor, followed by (iii) the light-excitation of the resulting radical anion (PC$^{•−}$) or radical cation (PC$^{•+}$, Scheme 38).
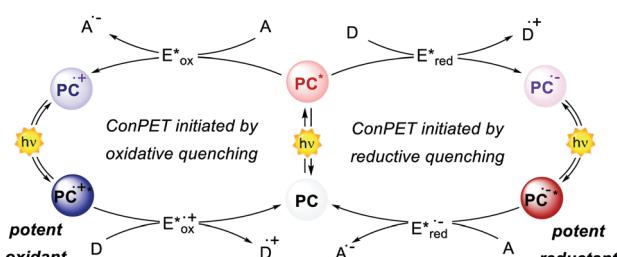


**Scheme 38** General catalytic manifolds of ConPET.
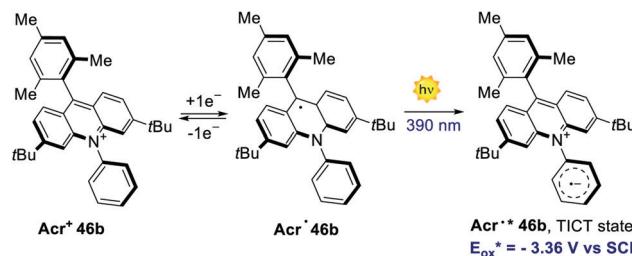


**Scheme 39** The strongly reducing radical Acr$^{••*}$ **46b**, formed upon the excitation of the acridium radical Acr$^{•}$ **46b**.

The requirement is that PC$^{•−}$ or PC$^{•+}$ to be further photo-excited must be sufficiently stable and long-lived, and the corresponding excited species are sufficiently long-lived (>1 ns) to allow the ET to happen.

Metal-based PCs have found a restricted use in ConPET cycles. Recent reports on the use of Ru and Ir complexes in two-photon photoredox cycles only involve the generation of highly reducing species in aqueous and/or micellar environments, with limited synthetic applicability.[81] On the contrary, organic PCs have demonstrated a much broader versatility both for thermodynamically challenging reduction and oxidation.

In 2020, Nicewicz's group documented the discovery, characterisation and reactivity of the excited acridine radical Acr$^{•*}$ **46b** (Scheme 39).[82] Spectroscopic and computational investigations revealed the formation of two main excited states for Acr$^{••*}$ **46b**, assigned as a lower-energy doublet (D$_1$) and a higher-energy twisted intramolecular charge-transfer state (TICT). The oxidation potentials of these excited states were estimated to be −2.91 V and −3.36 V vs. SCE, respectively, which are values comparable to those of elemental lithium ($E_{ox}$ (Li$^+$/Li$^0$) = −3.29 V). The singly occupied molecular orbital (SOMO) density of Acr$^{••*}$ **46b** was found to be localised on the acridine core, while the LUMO was placed on the N-phenyl ring. Further spectroscopical analysis with time-dependent density functional theory (TD-DFT) supported the formation of a charge-transfer state possessing both the aromatic radical anion and acridinium features, as it is expected for the proposed TICT state.

The reactivity of the highly reducing acridinium radical Acr$^{••*}$ **46b** was then demonstrated by the dehalogenation of aryl halides **84**, as well as by the desulfonylation of tosyl amines **85** (Scheme 40a). Both reduced products **86** and **87** were obtained in generally high yields (up to 98%) under optimised conditions. The scope of this process included substrates showing an $E_{red}$ up to −2.9 V, which are values not accessible to commonly used PCs. The proposed mechanism for the dehalogenation process involves the reductive quenching of the excited acridinium Acr$^{+*}$ **46b** by DIPEA **18**, generating the acridinium radical Acr$^{•}$ **46b** (Scheme 40b). This intermediate Acr$^{•}$ **46b** is then excited with a 390 nm light, populating both the highly reducing D$_n$ and TICT excited states (Acr$^{••*}$ **46b**). A single electron transfer subsequently occurs from Acr$^{••*}$ **46b** to the aryl halide **84**, forming the arene radical anion **84.1**, while regenerating Acr$^+$ **46b**. The intermediate **84.1** undergoes fragmentation, yielding the aryl radical **84.2**. Finally, a HAT

a)
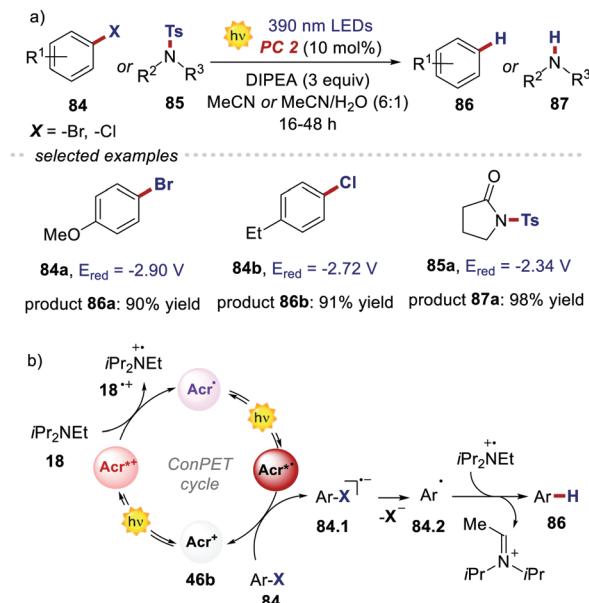


**Scheme 40** (a) Reductive dehalogenation of aryl halides (**81**) and reductive detosylation of amines (**82**) triggered by the excited radical acridinium Acr$^{\bullet\bullet}$**41b**. (b) The proposed mechanism for the dehalogenation of arenes.

event occurs for **84.2** from the amine radical cation **18$^{\bullet+}$**, which delivers the reduced product **86**.

On the other hand, two independent reports have exploited a ConPET manifold with PTH. In 2018, Wagenknecht's group realised the pentafluorosulfanylation/nucleophilic trapping of styrene derivatives through the use of UV and green light (Scheme 41).[83]

The highly reducing PTH* engages in oxidative quenching with SF$_6$, delivering SF$_5^{\bullet}$ and fluoride. The excitation of the poorly oxidising PTH$^{\bullet+}$ ($E_{ox}$ = 0.68 V) with green light transforms it into a powerful oxidant, which oxidises the thermodynamically demanding styrene derivative **88**. Coupling between SF$_5^{\bullet}$ and **88.1** affords the cationic intermediate **88.2**, which is then trapped by the nucleophilic fluoride ion. As a

result, PTH acts in the same photoredox cycle as a strong reductant for the reduction and fragmentation of SF$_6$ and as a strong oxidant for the oxidation of the styrene.

In 2021, Wickens's group realised the Nicewicz-type oxidative coupling between arenes **90** and N-heterocyclic nucleophile **91** through a similar ConPET manifold with PTH as the PC (Scheme 42).[84] In this case, oxygen serves as the electron acceptor to generate PTH$^{\bullet+}$ which, upon photoexcitation, can oxidise arenes with extreme oxidation potentials ($E_{ox}$ = 2.5 V for benzene).

Very recently, also 4CzIPN and its derivatives were used in ConPET cycles. Wickens's group realised the reductive defunctionalisation of electron-rich aryl chlorides **93** with 4DPAIPN and sodium formate as the electron donor.[85] Through the ConPET mechanism, the authors were able to reduce extremely challenging aryl chlorides **93** with reduction potentials as low as −3.4 V (Scheme 43).

Such a redox potential is beyond the thermodynamic limit accessible by a classic photoredox cycle under visible-light



**Scheme 42** (a) ConPET-enabled oxidative arene/N-heterocyclic nucleophile coupling. (b) The proposed mechanism.



**Scheme 41** (a) ConPET-enabled pentafluorosulfanylation/nucleophilic trapping of styrene derivatives. (b) The proposed mechanism.
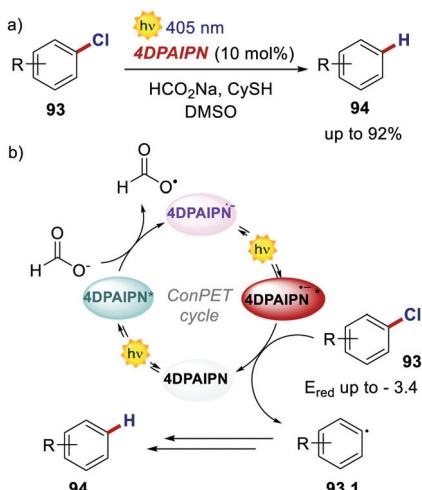


**Scheme 43** (a) Reductive defunctionalisation of electron-rich aryl chlorides. (b) Proposed reaction mechanism.
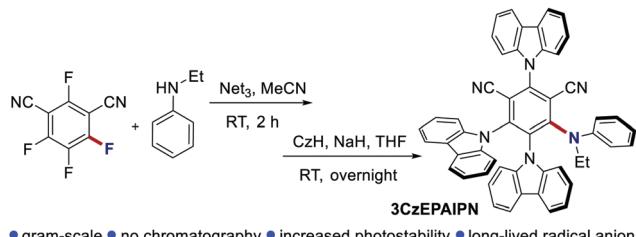
**Scheme 44** Synthesis and structure of 3CzEPAIPN.



**Fig. 7** Main advantages and open challenges associated with the use of IPN PCs.

irradiation. The authors also exploited the developed catalytic manifold for the phosphonylation, hydroarylation and borylation of aryl chlorides. However, complete suppression of the net reduction product **94** could not be achieved in such cases.

Similarly, Zhou and Wu's groups obtained the reductive borylation and phosphorylation of extremely challenging aryl chlorides through an analogous ConPET mechanism.[86] Key for the optimisation of the system was the use of 3CzEPAIPN, a modified derivative of 4CzIPN, as the PC (Scheme 44). Higher yields are attributed to the higher photostability of 3CzEPAIPN and the longer lifetime of its radical anion.

A catalytic platform for the activation of similarly demanding aryl chlorides was developed by Lambert and Lin's groups.[87] In this case, the radical anion of 9,10-dicyanoanthracene **3a** was produced by electrochemical reduction and was subsequently excited by blue light irradiation to yield a potent reductant ($E^{*\bullet-}_{red} = -3.2$ V *vs.* SCE).

These examples highlight the versatility of organic PCs in non-conventional multi-photon photoredox cycles. Through this strategy, it is possible to perform both thermodynamically challenging oxidation and reduction using the same organic PC.

# 7 Conclusions and future perspectives

Over the last decade, the field of organic photoredox catalysis has proven to have great potential to provide new synthetic methods under mild reaction conditions. Importantly, organic PCs are generally cheaper, less toxic and easier to modulate than transition metal PCs, thus representing a convenient and more sustainable alternative. In this feature article, we have outlined the evolution of the field of photoredox catalysis from the use of classical Ir- and Ru-complexes towards purely organic PCs. Remarkably, organic PCs can be efficiently used to replace their metal counterparts, while promoting previously inaccessible transformations. Their easy tunability also offers the possibility of building a large variety of structural and electronic variants and adopting a more rational PC selection. Recently, bimodal PCs, such as cyanoarenes (IPN scaffold), have become more and more popular thanks to their CT excited state character that mimics the MLCT of metal complexes, inferring long-lived excited states and a balanced distribution of the redox potentials (Fig. 7). However, the chemical stability of these PCs still represents an issue in the presence of highly nucleophilic radicals. König and co-workers demonstrated that 4CzIPN **78** can be *in situ* alkylated when
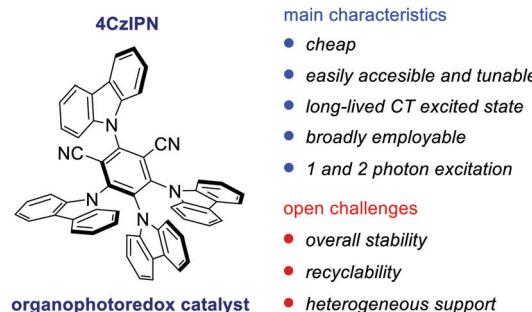
benzylic radicals are generated under reaction conditions (Scheme 36).

Our group has recently contributed to the field of organophotoredox catalysis by identifying naphtochromenone (NTC) PCs as a new class of bimodal organic PCs, with the ability to participate in both thermodynamically demanding oxidative and reductive photochemical processes. Interestingly, we have evaluated their stability and we were able to recover and reuse the NTC PC up to 5 times, maintaining virtually identical catalytic performances.[45] The recyclability of the PC is one important aspect often overlooked in academia, but may become essential towards industrial implementations. An additional open challenge regarding the possibility of supporting organic PCs is generating easily recoverable heterogeneous systems. This represents a complex issue, since solid supports can profoundly alter the ground and excited state properties of PCs, while introducing scattering problems.[88]

However, more sustainable reusable PCs,[89] having tuneable photochemical and redox properties, are needed to respond to the increasing demands of novel reactivity and bioactive molecules. To this end, novel structural variants must be evaluated, possibly unlocking new mechanistic paradigms. In particular, several heterocyclic scaffolds, which have already found applications as TADF emitters in OLEDs, have demonstrated interesting photochemical and redox properties.[90]

It is worth noting that while metal-based PCs have found a restricted use in only reductive ConPET cycles, organic PCs have instead exhibited a much broader versatility in both reductive and oxidative ConPET processes with PTH **31**, cyanoarenes and Acr-Mes$^+$ **46b** playing a central role.[82–86] This indicates that purely organic molecules will likely govern the evolution of the field. However, an unmet goal in ConPET processes is the use of the same PC class under both reductive and oxidative quenching. The possibility of using the same PC or PC class under both 1- and 2-photon thermodynamically opposite quenching mechanisms will represent a decisive advancement in terms of generality and versatility. In our group, we are currently evaluating this possibility with the use of a new generation of structurally robust NTC and IPN PCs.

Major discoveries are expected to come in the near future, given the new and broad opportunities that this class of relatively simple purely organic molecules can offer.

## Author contributions

T. B., S. C. and G. S. wrote the manuscript and drew the schemes and figures upon coordination by T. B. L. D. selected the topic and conceptualised the overall idea, directed the project, and corrected the text and the figures.

## Conflicts of interest

There are no conflicts to declare.

## Acknowledgements

## Notes and references

1 S. E. Braslavsky, *Pure Appl. Chem.*, 2007, **79**, 293–465.
2 H. D. Roth, *Angew. Chem., Int. Ed. Engl.*, 1989, **28**, 1193–1207.
3 G. Ciamician, *Science*, 1912, **36**, 385–394.
4 (a) D. Rehm and A. Weller, *Isr. J. Chem.*, 1970, **8**, 259–271; (b) L. Buzzetti, G. E. M. Crisenza and P. Melchiorre, *Angew. Chem., Int. Ed.*, 2019, **58**, 3730–3747.
5 For early examples on synthetic photoredox catalysis, see: (a) D. M. Hedstrand, W. H. Kruizinga and R. M. Kellogg, *Tetrahedron Lett.*, 1978, **19**, 1255–1258; (b) H. Cano-Yelo and A. Deronzier, *Tetrahedron Lett.*, 1984, **25**, 5517–5520; (c) H. Cano-Yelo and A. Deronzier, *J. Chem. Soc., Perkin Trans. 2*, 1984, 1093–1098; (d) H. Cano-Yelo and A. Deronzier, *J. Photochem.*, 1987, **37**, 315–321; (e) K. Okada, K. Okamoto and M. Oda, *J. Am. Chem. Soc.*, 1988, **110**, 8736–8738; (f) K. Okada, K. Okamoto, N. Morita, K. Okubo and M. Oda, *J. Am. Chem. Soc.*, 1991, **113**, 9401–9402; (g) K. Okada, K. Okubo, N. Morita and M. Oda, *Tetrahedron Lett.*, 1992, **33**, 7377–7380; (h) K. Okada, K. Okubo, N. Morita and M. Oda, *Chem. Lett.*, 1993, 2021–2024.
6 M. A. Ischay, M. E. Anzovino, J. Du and T. P. Yoon, *J. Am. Chem. Soc.*, 2008, **130**, 12886–12887.
7 D. A. Nicewicz and D. W. C. MacMillan, *Science*, 2008, **322**, 77–80.
8 J. M. R. Narayanam, J. W. Tucker and C. R. J. Stephenson, *J. Am. Chem. Soc.*, 2009, **131**, 8756–8757.
9 The results were obtained from a search on Elsevier Scopus using the keywords "photoredox catalyst" to obtain the total number of articles on the topic and "organic photoredox catalyst" for the number of articles on organophotoredox catalysis. The raw data were then refined to exclude reports that are not dealing with the use of photoredox catalysis for synthetic purposes. Despite this, it is possible that spurious results are still included, but they are expected to account for a non-significant fraction of the total.
10 (a) M. Graetzel, *Acc. Chem. Res.*, 1981, **14**, 376–384; (b) T. J. Meyer, *Acc. Chem. Res.*, 1989, **22**, 163–170.
11 H. Takeda and O. Ishitani, *Coord. Chem. Rev.*, 2010, **254**, 346–354.
12 C. R. Bock, J. A. Connor, A. R. Gutierrez, T. J. Meyer, D. G. Whitten, B. P. Sullivan and J. K. Nagle, *J. Am. Chem. Soc.*, 1979, **101**, 4815–4824.
13 K. A. King, P. J. Spellane and R. J. Watts, *J. Am. Chem. Soc.*, 1985, **107**, 1431–1432.
14 Selected photophysical studies: (a) W. J. Finkenzeller and H. Yersin, *Chem. Phys. Lett.*, 2003, **377**, 299–305; (b) T. Hofbeck and H. Yersin, *Inorg. Chem.*, 2010, **49**, 9290–9299For a comprehensive review, see: (c) H. Yersin, A. F. Rausch, R. Czerwieniec, T. Hofbeck and T. Fischer, *Coord. Chem. Rev.*, 2011, **255**, 2622–2652.
15 For comprehensive reviews on the photophysical properties of iridium and ruthenium complexes, see: (a) L. Flamigni, A. Barbieri, C. Sabatini, B. Ventura and F. Barigelletti, in *Photochemistry and Photophysics of Coordination Compounds II*, ed. V. Balzani and S. Campagna, Springer, Berlin Heidelberg, 2007,

ch. 4, vol. 281, pp. 143–203 For ruthenium, see; (b) S. Campagna, F. Puntoriero, F. Nastasi, G. Bergamini and V. Balzani, in *Photochemistry and Photophysics of Coordination Compounds II*, ed. V. Balzani and S. Campagna, Springer, Berlin Heidelberg, 2007, ch. 4, vol. 280, pp. 117–214 For reviews on the use of photoactive metal complexes in organic synthesis, see; (c) C. K. Prier, D. A. Rankic and D. W. C. MacMillan, *Chem. Rev.*, 2013, **113**, 5322–5363; (d) K. Teegardin, J. I. Day, J. Chan and J. Weaver, *Org. Process Res. Dev.*, 2016, **20**, 1156–1163; (e) J.-H. Shon and T. S. Teets, *Comments Inorg. Chem.*, 2020, **40**, 53–85; (f) J. M. R. Narayanam and C. R. J. Stephenson, *Chem. Soc. Rev.*, 2011, **40**, 102–113; (g) M. Reckenthäler and A. G. Griesbeck, *Adv. Synth. Catal.*, 2013, **355**, 2727–2744; (h) K. L. Skubi, T. R. Blum and T. P. Yoon, *Chem. Rev.*, 2016, **116**, 10035–10074; (i) J. Twilton, C. Le, P. Zhang, M. H. Shaw, R. W. Evans and D. W. C. MacMillan, *Nat. Chem. Rev.*, 2017, **1**, 0052; (j) F. Glaser and O. S. Wenger, *Coord. Chem. Rev.*, 2020, **405**, 213129.
16 For selected examples on tailored Ir complexes able to operate under reductive quenching, see: (a) D. A. Nagib, M. E. Scott and D. W. C. MacMillan, *J. Am. Chem. Soc.*, 2009, **131**, 10875–10877; (b) A. G. Condie, J. C. González-Gómez and C. R. J. Stephenson, *J. Am. Chem. Soc.*, 2010, **132**, 1464–1465; (c) J. W. Tucker, J. D. Nguyen, J. M. R. Narayanam, S. W. Krabbe and C. R. J. Stephenson, *Chem. Commun.*, 2010, **46**, 4985–4987; (d) E. B. Corcoran, M. T. Pirnot, S. Lin, S. D. Dreher, D. A. DiRocco, I. W. Davies, S. L. Buchwald and D. W. C. MacMillan, *Science*, 2016, **353**, 279–283.
17 For the synthesis of tailored Ir complexes, see: M. S. Lowry, J. I. Goldsmith, J. D. Slinker, R. Rohl, R. A. Pascal, G. G. Malliaras and S. Bernhard, *Chem. Mater.*, 2005, **17**, 5712–5719.
18 (a) D. P. Rillema, G. Allen, T. J. Meyer and D. Conrad, *Inorg. Chem.*, 1983, **22**, 1617–1622; (b) M. Haga, E. S. Dodsworth, G. Eryavec, P. Seymour and A. B. P. Lever, *Inorg. Chem.*, 1985, **24**, 1901–1906.
19 E. D. Nacsa and D. W. C. MacMillan, *J. Am. Chem. Soc.*, 2018, **140**, 3322–3330.
20 K. Dedeian, P. I. Djurovich, F. O. Garces, G. Carlson and R. J. Watts, *Inorg. Chem.*, 1991, **30**, 1685–1687.
21 W. M. Haynes, *CRC Handbook of Chemistry and Physics*, CRC Press, Boca Raton, 2014.
22 *Nat. Catal.*, 2019, **2**, 735.
23 P. Chábera, K. S. Kjaer, O. Prakash, A. Honarfar, Y. Liu, L. A. Fredin, T. C. B. Harlang, S. Lidin, J. Uhlig, V. Sundström, R. Lomoth, P. Persson and K. Wärnmark, *J. Phys. Chem. Lett.*, 2018, **9**, 459–463.
24 (a) B. M. Hockin, C. Li, N. Robertson and E. Zysman-Colman, *Catal. Sci. Technol.*, 2019, **9**, 889–915; (b) S. Paria and O. Reiser, in *Visible Light Photocatalysis in Organic Chemistry*, ed. C. Stephenson, T. Yoon and D. W. C. MacMillan, Wiley-VCH, Weinheim, 2018, ch. 7, pp. 233–251; (c) G. Noirbent and F. Dumur, *Catalysts*, 2020, **10**, 953.
25 For selected reviews, see: (a) S. Fukuzumi and K. Ohkubo, *Org. Biomol. Chem.*, 2014, **12**, 6059–6071; (b) D. P. Hari and B. König, *Chem. Commun.*, 2014, **50**, 6688–6699; (c) N. A. Romero and D. A. Nicewicz, *Chem. Rev.*, 2016, **116**, 10075–10166; (d) Y. Du, R. M. Pearson, C.-H. Lim, S. M. Sartor, M. D. Ryan, H. Yang, N. H. Damrauer and G. M. Miyake, *Chem. – Eur. J.*, 2017, **23**, 10962–10968; (e) T.-Y. Shang, L.-H. Lu, Z. Cao, Y. Liu, W.-M. He and B. Yu, *Chem. Commun.*, 2019, **55**, 5408–5419; (f) S. G. E. Amos, M. Garreau, L. Buzzetti and J. Waser, *Beilstein J. Org. Chem.*, 2020, **16**, 1163–1187; (g) P. P. Singh and V. Srivastava, *Org. Biomol. Chem.*, 2021, **19**, 313–321; (h) Y. Lee and M. S. Kwon, *Eur. J. Org. Chem.*, 2020, 6028–6043; (i) M. V. Bobo, J. J. Kuchta and A. K. Vannucci, *Org. Biomol. Chem.*, 2021, **19**, 4816–4834; (j) M. A. Bryden and E. Zysman-Colman, *Chem. Soc. Rev.*, 2021, **50**, 7587–7680; (k) A. Tlili and S. Lakhdar, *Angew. Chem., Int. Ed.*, 2021, **60**, 19526–19549; (l) Y. Wu, D. Kim and T. S. Teets, *Synlett*, 2021, DOI: 10.1055/a-1390-9065.
26 (a) A. Joshi-Pangu, F. Lévesque, H. G. Roth, S. F. Oliver, L.-C. Campeau, D. Nicewicz and D. A. DiRocco, *J. Org. Chem.*, 2016, **81**, 7244–7249; (b) B. G. McCarthy, R. M. Pearson, C.-H. Lim, S. M. Sartor, N. H. Damrauer and G. M. Miyake, *J. Am. Chem. Soc.*, 2018, **140**, 5088–5101; (c) E. Speckmeier, T. G. Fischer and K. Zeitler, *J. Am. Chem. Soc.*, 2018, **140**, 15353–15365; (d) A. Vega-Peñaloza, J. Mateos, X. Companyó, M. Escudero-Casao and L. Dell'Amico, *Angew. Chem., Int. Ed.*, 2021, **60**, 1082–1097.
27 F. Strieth-Kalthoff, M. J. James, M. Teders, L. Pitzer and F. Glorius, *Chem. Soc. Rev.*, 2018, **47**, 7190–7202.

28 At the same time, however, the stabilisation of the CT state in polar solvents produces a redshift in the emission (Stokes shift), lowering the energy of the excited state and reducing the redox potential window.

29 M. V. Bobo, A. M. Arcidiacono, P. J. Ayare, J. C. Reed, M. R. Helton, T. Ngo, K. Hanson and A. K. Vannucci, ChemPhotoChem, 2021, 5, 51–57.

30 K. Zeitler, in Visible Light Photocatalysis in Organic Chemistry, ed. C. Stephenson, T. Yoon and D.W.C. MacMillan, Wiley-VCH, Weinheim, 2018, ch. 6, pp. 159–232.

31 (a) A. Penzkofer, A. Beidoun and M. Daiber, J. Lumin., 1992, 51, 297–314; (b) A. Penzkofer and A. Beidoun, Chem. Phys., 1993, 177, 203–216; (c) A. Penzkofer, A. Beidoun and S. Speiser, Chem. Phys., 1993, 170, 139–148.

32 M. E. Selsted and H. W. Becker, Anal. Biochem., 1986, 155, 270–274.

33 (a) A. Chisvert and A. Salvador, in Analysis of Cosmetic Products, ed. A. Salvador and A. Chisvert, Elsevier, Amsterdam, 2nd edn, 2018, ch. 5, pp. 85–106; (b) R. W. Sabnis, Handbook of Biological Dyes and Stains, John Wiley & Sons, Inc., Hoboken, 2010.

34 R. W. Sabnis, Handbook of Acid-Base Indicators, CRC Press, Boca Raton, 2007.

35 M. Neumann, S. Füldner, B. König and K. Zeitler, Angew. Chem., Int. Ed., 2011, 50, 951–954.

36 M. A. Cismesia and T. P. Yoon, Chem. Sci., 2015, 6, 5426–5434.

37 J. Du, L. R. Espelt, I. A. Guzei and T. P. Yoon, Chem. Sci., 2011, 2, 2115–2119.

38 M. Neumann and K. Zeitler, Chem. – Eur. J., 2013, 19, 6950–6955.

39 S. P. Pitre, C. D. McTiernan, H. Ismaili and J. C. Scaiano, J. Am. Chem. Soc., 2013, 135, 13286–13289.

40 (a) T. Ohno and N. N. Lichtin, J. Am. Chem. Soc., 1980, 102, 4636–4643; (b) R. H. Kayser and R. H. Young, Photochem. Photobiol., 1976, 24, 395–401; (c) H.-J. Timpe and S. Neuenfeld, J. Chem. Soc., Faraday Trans., 1992, 88, 2329–2336; (d) T. Shen, Z.-G. Zhao, Q. Yu and H.-J. Xu, J. Photochem. Photobiol., A, 1989, 47, 203–212.

41 (a) F. Wilkinson, W. P. Helman and A. B. Ross, J. Phys. Chem. Ref. Data, 1995, 24, 663–677; (b) C. Tanielian and C. Wolff, J. Phys. Chem., 1995, 99, 9831–9837.

42 Y. Q. Zou, J. R. Chen, X. P. Liu, L. Q. Lu, R. L. Davis, K. A. Jørgensen and W. J. Xiao, Angew. Chem., Int. Ed., 2012, 51, 784–788.

43 (a) L. Mei, J. M. Veleta and T. L. Gianetti, J. Am. Chem. Soc., 2020, 142, 12056–12061For the synthesis of the precursors of PC 19, see: (b) B. Laursen and F. Krebs, Angew. Chem., Int. Ed., 2000, 39, 3432–3434; (c) J. C. Martin and Russell G. Smith, J. Am. Chem. Soc., 1964, 86, 2252–2256.

44 D. Kalyani, K. B. McMurtrey, S. R. Neufeldt and M. S. Sanford, J. Am. Chem. Soc., 2011, 133, 18566–18569.

45 J. Mateos, F. Rigodanza, A. Vega-Peñaloza, A. Sartorel, M. Natali, T. Bortolato, G. Pelosi, X. Companyó, M. Bonchio and L. Dell'Amico, Angew. Chem., Int. Ed., 2020, 59, 1302–1312.

46 J. Mateos, N. Meneghini, M. Bonchio, N. Marino, T. Carofiglio, X. Companyó and L. Dell'Amico, Beilstein J. Org. Chem., 2018, 14, 2418–2424.

47 (a) X. Ju, D. Li, W. Li, W. Yu and F. Bian, Adv. Synth. Catal., 2012, 354, 3561–3567; (b) Z. Liang, S. Xu, W. Tian and R. Zhang, Beilstein J. Org. Chem., 2015, 11, 425–430.

48 K. Matyjaszewski, Macromolecules, 2012, 45, 4015–4039.

49 V. K. Singh, C. Yu, S. Badgujar, Y. Kim, Y. Kwon, D. Kim, J. Lee, T. Akhter, G. Thangavel, L. S. Park, J. Lee, P. C. Nandajan, R. Wannemacher, B. Milián-Medina, L. Lüer, K. S. Kim, J. Gierschner and M. S. Kwon, Nat. Catal., 2018, 1, 794–804.

50 G. Zhang, Y. Song, K. H. Ahn, T. Park and W. Choi, Macromolecules, 2011, 44, 7594–7599.

51 B. P. Fors and C. J. Hawker, Angew. Chem., Int. Ed., 2012, 51, 8850–8853.

52 (a) N. J. Treat, H. Sprafke, J. W. Kramer, P. G. Clark, B. E. Barton, J. Read de Alaniz, B. P. Fors and C. J. Hawker, J. Am. Chem. Soc., 2014, 136, 16096–16101; (b) G. M. Miyake and J. C. Theriot, Macromolecules, 2014, 47, 8255–8261.

53 E. H. Discekici, N. J. Treat, S. O. Poelma, K. M. Mattson, Z. M. Hudson, Y. Luo, C. J. Hawker and J. R. de Alaniz, Chem. Commun., 2015, 51, 11705–11708.

54 J. D. Nguyen, E. M. D'Amato, J. M. R. Narayanam and C. R. J. Stephenson, Nat. Chem., 2012, 4, 854–859.

55 (a) C. D. McTiernan, S. P. Pitre and J. C. Scaiano, ACS Catal., 2014, 4, 4034–4039; (b) E. Arceo, E. Montroni and P. Melchiorre, Angew. Chem., Int. Ed., 2014, 53, 12064–12068.

56 C. B. Tripathi, T. Ohtani, M. T. Corbett and T. Ooi, Chem. Sci., 2017, 8, 5622–5627.

57 L. J. Allen, P. J. Cabrera, M. Lee and M. S. Sanford, J. Am. Chem. Soc., 2014, 136, 5607–5610.

58 L. Chu, C. Ohta, Z. Zuo and D. W. C. MacMillan, J. Am. Chem. Soc., 2014, 136, 10886–10889.

59 S. Fukuzumi, H. Kotani, K. Ohkubo, S. Ogo, N. V. Tkachenko and H. Lemmetyinen, J. Am. Chem. Soc., 2004, 126, 1600–1601.

60 (a) D. S. Hamilton and D. A. Nicewicz, J. Am. Chem. Soc., 2012, 134, 18577–18580; (b) N. A. Romero, K. A. Margrey, N. E. Tay and D. A. Nicewicz, Science, 2015, 349, 1326–1330; (c) W. P. Hess and F. P. Tully, J. Phys. Chem., 1989, 93, 1944–1947.

61 For selected examples on the reducing ability of acridinium ions, see: (a) M. Xiang, Z.-K. Xin, B. Chen, C.-H. Tung and L.-Z. Wu, Org. Lett., 2017, 19, 3009–3012; (b) M. Xiang, C. Zhou, X.-L. Yang, B. Chen, C.-H. Tung and L.-Z. Wu, J. Org. Chem., 2020, 85, 9080–9087.

62 H. G. Roth, N. A. Romero and D. A. Nicewicz, Synlett, 2016, 714–723.

63 (a) T. M. Nguyen and D. A. Nicewicz, J. Am. Chem. Soc., 2013, 135, 9588–9591; (b) A. J. Perkowski and D. A. Nicewicz, J. Am. Chem. Soc., 2013, 135, 10334–10337; (c) D. J. Wilger, J.-M. M. Grandjean, T. R. Lammert and D. A. Nicewicz, Nat. Chem., 2014, 6, 720–726; (d) N. A. Romero and D. A. Nicewicz, J. Am. Chem. Soc., 2014, 136, 17024–17035.

64 D. A. Armstrong, Q. Sun and R. H. Schuler, J. Phys. Chem., 1996, 100, 9892–9899.

65 K. Ohkubo, K. Mizushima, R. Iwata, K. Souma, N. Suzuki and S. Fukuzumi, Chem. Commun., 2010, 46, 601–603.

66 (a) N. E. S. Tay and D. A. Nicewicz, J. Am. Chem. Soc., 2017, 139, 16100–16104; (b) W. Chen, Z. Huang, N. E. S. Tay, B. Giglio, M. Wang, H. Wang, Z. Wu, D. A. Nicewicz and Z. Li, Science, 2019, 364, 1170–1174; (c) N. Holmberg-Douglas, N. P. R. Onuska and D. A. Nicewicz, Angew. Chem., Int. Ed., 2020, 59, 7425–7429.

67 (a) C. Fischer and C. Sparr, Angew. Chem., Int. Ed., 2018, 57, 2436–2440; (b) C. Fischer and C. Sparr, Tetrahedron, 2018, 74, 5486–5493; (c) B. Zilate, C. Fischer, L. Schneider and C. Sparr, Synthesis, 2019, 4359–4365; (d) A. Gini, M. Uygur, T. Rigotti, J. Alemán and O. García Mancheño, Chem. – Eur. J., 2018, 24, 12509–12514; (e) A. R. White, L. Wang and D. A. Nicewicz, Synlett, 2019, 827–832; (f) C. Fischer, C. Kerzig, B. Zilate, O. S. Wenger and C. Sparr, ACS Catal., 2020, 10, 210–215.

68 Z. Zuo, D. T. Ahneman, L. Chu, J. A. Terrett, A. G. Doyle and D. W. C. MacMillan, Science, 2014, 345, 437–440.

69 (a) J. C. Theriot, C. H. Lim, H. Yang, M. D. Ryan, C. B. Musgrave and G. M. Miyake, Science, 2016, 352, 1082–1086; (b) R. M. Pearson, C. H. Lim, B. G. McCarthy, C. B. Musgrave and G. M. Miyake, J. Am. Chem. Soc., 2016, 138, 11399–11407; (c) B. L. Buss, C. H. Lim and G. M. Miyake, Angew. Chem., Int. Ed., 2020, 59, 3209–3217; (d) N. A. Swisher, D. A. Corbin and G. M. Miyake, ACS Macro Lett., 2021, 10, 453–459.

70 A. L. Berger, K. Donabauer and B. König, Chem. Sci., 2018, 9, 7230–7235.

71 D. B. Vogt, C. P. Seath, H. Wang and N. T. Jui, J. Am. Chem. Soc., 2019, 141, 13203–13211.

72 M. H. Shaw, J. Twilton and D. W. C. MacMillan, J. Org. Chem., 2016, 81, 6898–6926.

73 L. Capaldo, R. Riccardi, D. Ravelli and M. Fagnoni, ACS Catal., 2018, 8, 304–309.

74 N. Bortolamei, A. A. Isse and A. Gennaro, Electrochim. Acta, 2010, 55, 8312–8318.

75 H. Uoyama, K. Goushi, K. Shizu, H. Nomura and C. Adachi, Nature, 2012, 492, 234–238.

76 J. Luo and J. Zhang, ACS Catal., 2016, 6, 873–877.

77 Q.-Y. Meng, T. E. Schirmer, A. L. Berger, K. Donabauer and B. König, J. Am. Chem. Soc., 2019, 141, 11393–11397.

78 T. Duhail, T. Bortolato, J. Mateos, E. Anselmi, B. Jelier, A. Togni, E. Magnier, G. Dagousset and L. Dell'Amico, Org. Lett., 2021, 23, 7088–7093.

79 B. J. Jelier, P. F. Tripet, E. Pietrasiak, I. Franzoni, G. Jeschke and A. Togni, Angew. Chem., Int. Ed., 2018, 57, 13784–13789.

80 I. Ghosh, T. Ghosh, J. I. Bardagi and B. König, Science, 2014, 346, 725–728.

81 (a) R. Naumann, F. Lehmann and M. Goez, Chem. – Eur. J., 2018, 24, 13259–13269; (b) R. Naumann and M. Goez, Chem. – Eur. J., 2018, 24,

9833–9840; (c) R. Naumann and M. Goez, *Chem. – Eur. J.*, 2018, **24**, 17557–17567; (d) C. Kerzig, X. Guo and O. S. Wenger, *J. Am. Chem. Soc.*, 2019, **141**, 2122–2127; (e) M. Giedyk, R. Narobe, S. Weiß, D. Touraud, W. Kunz and B. König, *Nat. Catal.*, 2020, **3**, 40–47.

82 I. A. MacKenzie, L. Wang, N. P. R. Onuska, O. F. Williams, K. Begam, A. M. Moran, B. D. Dunietz and D. A. Nicewicz, *Nature*, 2020, **580**, 76–80.

83 D. Rombach and H.-A. Wagenknecht, *ChemCatChem*, 2018, **10**, 2955–2961.

84 K. Targos, O. P. Williams and Z. K. Wickens, *J. Am. Chem. Soc.*, 2021, **143**, 4125–4132.

85 A. F. Chmiel, O. P. Williams, C. P. Chernowsky, C. S. Yeung and Z. K. Wickens, *J. Am. Chem. Soc.*, 2021, **143**, 10882–10889.

86 J. Xu, J. Cao, X. Wu, H. Wang, X. Yang, X. Tang, R. W. Toh, R. Zhou, E. K. L. Yeow and J. Wu, *J. Am. Chem. Soc.*, 2021, **143**, 13266–13273.

87 H. Kim, H. Kim, T. H. Lambert and S. Lin, *J. Am. Chem. Soc.*, 2020, **142**, 2087–2092.

88 M. Melchionna and P. Fornasiero, *ACS Catal.*, 2020, **10**, 5493–5501.

89 B. Bartolomei, G. Gentile, C. Rosso, G. Filippini and M. Prato, *Chem. – Eur. J.*, 2021, **27**, 16062–16070.

90 (a) T. Serevičius, T. Nakagawa, M.-C. Kuo, S.-H. Cheng, K.-T. Wong, C.-H. Chang, R. C. Kwong, S. Xiae and C. Adachi, *Phys. Chem. Chem. Phys.*, 2013, **15**, 15850–15855; (b) C. Tang, R. Bi, Y. Tao, F. Wang, X. Cao, S. Wang, T. Jiang, C. Zhong, H. Zhang and W. Huang, *Chem. Commun.*, 2015, **51**, 1650–1653.